

Evidence That *Dmrta2* Acts through Repression of *Pax6* in Cortical Patterning and Identification of a Mutation Impairing DNA Recognition Associated with Microcephaly in Human

Xueyi Shen,¹ Jithu Anirudhan,^{1*} Ambrin Fatima,^{2*} Estelle Plant,^{3*} Tünde Szemes,¹ Zélie Bouveret,⁴ Marc Keruzore,¹ Sadia Kricha,¹ Xinsheng Nan,⁵ Alba Sabaté San José,¹ Samuel Bianchin,¹ Bérénice Veraghen,¹ Louis-Paul Delhayé,¹ Bilal Ahmad Mian,² Lubaba Binte Khalid,² Farhan Ali,⁶ Hijab Zahra,² Asmat Ali,² Mathias Toft,^{7,8} Marc Dieu,⁹ Younes Achouri,¹⁰ Meng Li,⁵ Patricia Renard,⁹ Carine Van Lint,³ Coralie Poulard,⁴ Zafar Iqbal,⁶ and Eric J. Bellefroid¹

¹Laboratory of Developmental Genetics, Department of Molecular Biology and ULB Neuroscience Institute (UNI), Université Libre de Bruxelles, Gosselies 6041, Belgium, ²Department of Biological and Biomedical Sciences, Aga Khan University, Karachi 74800, Pakistan, ³Service of Molecular Virology, Department of Molecular Biology and ULB-Cancer Research Centre, Université Libre de Bruxelles, Gosselies 6041, Belgium, ⁴INSERM U1052, CNRS UMR5286, Université Claude Bernard Lyon1, Centre de Recherche en Cancérologie de Lyon, Lyon F-69000, France, ⁵Neuroscience and Mental Health Research Institute, School of Medicine, Cardiff University, Cardiff CF24 4HQ, United Kingdom, ⁶Department of Paediatrics and Child Health, Aga Khan University, Karachi 74800, Pakistan, ⁷Department of Neurology, Oslo University Hospital, Oslo 0424, Norway, ⁸Institute of Clinical Medicine, University of Oslo, Oslo 0424, Norway, ⁹MaSUN-Proteomic Facility, Université de Namur, Namur 5000, Belgium, and ¹⁰Transgene Technology Platform TRSG, Université catholique de Louvain, Leuven 1348, Belgium

Received Aug. 15, 2024; revised March 27, 2025; accepted April 15, 2025.

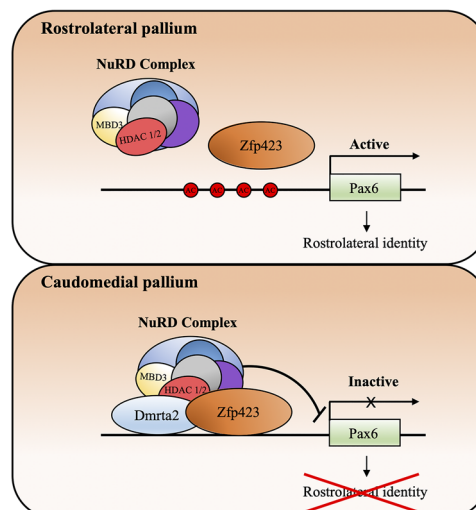
The authors declare no competing financial interests.

Author contributions: E.J.B. designed research; X.S., J.A., T.S., M.K., A.S.S.J., S.K., L-P.D., E.P., P.R., M.D., Y.A., M.T., A.F., B.A.M., L.B.K., F.A., H.Z., A.A., C.P., X.N., Z.B., S.B., and B.V. performed research; J.A., T.S., A.S.S.J., S.K., and L-P.D. contributed unpublished reagents/analytic tools; E.J.B., X.S., J.A., T.S., M.K., A.S.S.J., C.V.L., E.P., P.R., M.D., Z.I., A.F., X.N., and B.V. analyzed data; E.J.B., X.S., Z.I., C.P., M.L., X.N., and S.B. wrote the paper.

We thank Dr. Noriko Osumi for the *Pax6*^{Sey/+} mice, Dr. Ulriche Teichman for the pJoP6 mice, and Dr. Vassiliki Fotaki for the *BAT-GAL* mice. We also thank Dr. Dirk Kleinjan for providing us with a mouse BAC clone containing the *Pax6* E60 enhancer, Dr. Croci Laura for providing us with a *Zfp423* expression plasmid, and Dr. David Zarkow for helpful discussions.

Continued on next page.

Visual Abstract



Abstract

Dmrt2 (also designated *Dmrt5*) is a transcriptional regulator expressed in cortical progenitors in a caudomedial^{high}/rostralateral^{low} gradient with important roles at different steps of cortical development. *Dmrt2* has been suggested to act in cortex development mainly by differential suppression of *Pax6* and other homeobox transcription factors such as the ventral telencephalic regulator *Gsx2*, which remains to be fully demonstrated. Here we have addressed the epistatic relation between *Pax6* and *Dmrt2* by comparing phenotypes in mutant embryos or embryos overexpressing both genes in various allelic combinations. We show that *Dmrt2* cooperates with *Pax6* in the maintenance of cortical identity in dorsal telencephalic progenitors and that it acts as a transcriptional repressor of *Pax6* to control cortical patterning. Mechanistically, we show that in P19 cells, *Dmrt2* acts as a DNA binding-dependent repressor on the *Pax6 E60* enhancer and that a point mutation that affects its DNA binding properties identified in a consanguineous family leads to agenesis of the corpus callosum, pachygyria, and the absence of the cingulate gyrus. Finally, we provide evidence that *Dmrt2* binds components of the NuRD repressor complex and interacts with zinc finger proteins such as *Zfp423*. Together, our results highlight the importance and conserved function of *Dmrt2* in cortical development and provide novel insights into its mechanism of action.

Key words: cerebral cortex; microcephaly; neural progenitor; neurogenesis; patterning; transcription factor

Significance Statement

Cortico-genesis is controlled by an array of transcription factors that coordinate neural progenitor self-renewal and differentiation to generate correct cortical cell number and diversity. However, how this complex array of transcription factors works in concert to regulate this process remains largely unknown. Here we provide insights into the mechanism of action of the transcription factor *Dmrt2* by demonstrating that it cooperates with *Pax6* to define the pallium-subpallium boundary and acts by repressing it to control cortical patterning. Our data also reveal that *Dmrt2* interacts with components of the NuRD repressor complex and with the *Zfp423* zinc finger protein and that a point mutation that affects its DNA binding causes cortical abnormalities in human, further highlighting its importance in cortex development.

Introduction

Balancing neural progenitor self-renewal and differentiation is essential for generating cells in correct numbers and diverse types during neural development. During cerebral cortex development, neurogenesis is tightly regulated by a complex array of transcription factors (TFs). Many of these TFs are expressed in graded patterns along the rostral/caudal (R/C) and dorsal/ventral (D/V) axes of the developing ventricular zone (VZ) of the pallium (dorsal telencephalon) under the control of signals produced by localized signaling centers located at the periphery of the cortical primordium (Cadwell et al., 2019; Tole and Hébert, 2020; Ypsilanti et al., 2021). How this host of TFs expressed in gradients in progenitors orchestrates together their proliferation and differentiation to build the cerebral cortex remains today an important unanswered question.

Among the genes coding for cortical TFs is the zinc finger *Dmrt2* gene, also named *Dmrt5*, which is expressed in a caudomedial^{high}/rostralateral^{low} gradient in the developing cortical VZ. In mice lacking *Dmrt2*, the telencephalic vesicle size is decreased due to premature differentiation of progenitors (Young et al., 2017). The hippocampus and the cortical hem, one of the major telencephalic patterning centers, and the caudal neocortical area are strongly reduced (Konno et al., 2012; Saulnier et al., 2013). The additional knock-out of the related *Dmrt3* gene in mice lacking *Dmrt2* leads to a more severe phenotype with cortical progenitors expressing ventral telencephalic markers such as *Gsx2* (Desmaris et al., 2018). Conditional deletion of *Dmrt2* leaving cortical hem intact also results in a similar phenotype, suggesting that *Dmrt2* controls the patterning of the cortex independently of its influence on the hem. Conversely, in *Dmrt2* overexpressing mice, the caudal area expands while rostral ones are reduced (De Clercq et al., 2018).

*J.A., A.F., and E.P. contributed equally to this work.

This work was supported by the FNRS (CDR J001121F) and the Internationale Brachet Stiftung (IBS) to E.J.B. X.S. was a China Scholarship Council fellow and obtained a "Fondation Rose et Jean Hoguet" fellowship. J.A. was an FNRS-FRIA fellow and obtained a "Fonds David and Alice Van Buuren" fellowship. T.S. was a ULB-UMons fellow, and A.S.S.J and S.B. FNRS fellows. Z.I. was supported by a grant from the South-Eastern Norway Regional Health Authority. C.V.L. acknowledges funding from the Belgian National Fund for Scientific Research (F.R.S-FNRS, Belgium) and the Internationale Brachet Stiftung (IBS). E.P. was funded by fellowships from The Télévie program of the F.R.S-FNRS, the "Fondation Rose et Jean Hoguet", Apex Biosolutions, and then the French INSERM agency "ANRS/Maladies infectieuses émergentes". C.V.L. is "Directrice de Recherches" of the F.R.S-FNRS.

Correspondence should be addressed to Zafar Iqbal at zafar.iqbal@ous-research.no or Eric J. Bellefroid at Eric.Bellefroid@ulb.be.

Copyright © 2025 Shen et al.
This is an open-access article distributed under the terms of the [Creative Commons Attribution 4.0 International license](https://creativecommons.org/licenses/by/4.0/), which permits unrestricted use, distribution and reproduction in any medium provided that the original work is properly attributed.

Mechanistically, *Dmrt2* has been shown to bind to telencephalic enhancers of the *Pax6* and *Gsx2* loci and repress their expression (Konno et al., 2019). While both *Dmrt2* and *Pax6* contribute to telencephalic dorsoventral patterning by repressing ventral telencephalic-specific genes, *Pax6* within cortical progenitors regulates in an opposite manner to *Dmrt2* patterning and arealization of the neocortex (Ypsilanti and Rubenstein, 2016). Although *Pax6* effects are context and dose dependent, it can promote neuronal differentiation while *Dmrt2* promotes the maintenance of neural progenitors during neurogenesis (Manuel et al., 2015; Young et al., 2017). Therefore, it has been suggested that *Dmrt2* acts through the repression of *Gsx2* to define the dorsal telencephalic compartment and through the repression of *Pax6* to determine positional information within cortical progenitors (Konno et al., 2019). First evidence for the hypothesis that *Dmrt2* acts through *Pax6* in cortex development has been obtained in *Dmrt2* loss of function experiments using electroporated siRNA, in the context of its opposite function to *Pax6* in the control of the differentiation of progenitors. Results obtained showed that the double knockdown of *Dmrt3* and *Dmrt2* upregulates the expression of proneural genes such as *Neurog2* or *Neurod1* that act as the primary initiators of neuronal differentiation and are directly activated by *Pax6*, while the additional knockdown of *Pax6* in *Dmrt3*; *Dmrt2* double knockdown rescued the neurogenic phenotype (Konno et al., 2019).

In this study, we compared phenotypes of mutant embryos for both *Dmrt2* and *Pax6* with transgenics overexpressing only *Dmrt2* to understand how *Dmrt2* and *Pax6* function together in cortex development. We then performed reporter assays in P19 teratocarcinoma cells and rapid immunoprecipitation followed by mass spectrometry of endogenous protein (RIME) experiments to approach the mechanism of action of *Dmrt2*. We also examined in human a novel case of microcephaly with a point mutation in *DMRTA2*. Together, our results demonstrate the importance of *Dmrt2* and *Pax6* interactions in the positional information of cortical progenitors and provide first insights into its mechanism of action.

Materials and Methods

Ethics statement. The animal experimental procedures were approved by the CEBEA (Comité d'éthique et du bien-être animal) of the IBMM (Institut de Biologie et de Médecine Moléculaires) -ULB and conformed to the European guidelines on the ethical care and use of animals.

Animal lines and genotyping. The mid-day of the vaginal plug discovery was termed embryonic day 0.5 (E0.5), and the first 24 h (h) after birth was postnatal day (P) 0. Mice were provided *ad libitum* with standard mouse lab pellet food and water and housed at room temperature (RT) with a 12 h light/dark cycle.

Dmrt2^{+/-} and *Dmrt2*^{Tg/+} (De Clercq et al., 2018), *Pax6*^{sey/+} (Hill et al., 1991), and *BAT-gal* (Maretto et al., 2003) mice were maintained in a C57Bl/6 background. *Pax6*^{Tg/+} (Berger et al., 2007) were in an FVB/N background. The *Dmrt2* knock-in (*Dmrt2*^{2xHA}) mouse line was generated using CRISPR/cas9 editing. A crRNA was designed using CRISPRdirect (<http://crispr.dbcls.jp/>) with the intent to produce a double-strand break in the second exon of *Dmrt2*, 5' from the ATG codon. 2.4 pmol/μl of annealed crRNA (10 nmol, Integrated DNA Technologies, 5'-TCCAGCCATG GAGCTGCGCT-3') and the tracrRNA (Integrated DNA Technologies, catalog #1072534) were injected into fertilized egg with 100 ng/μl of recombinant Cas9 protein (Integrated DNA Technologies) and 10 ng/μl of a single single-stranded DNA oligonucleotide template with homology arms to the targeted region and containing a 2XHA sequence (Integrated DNA Technologies, Megamer ssDNA Fragment: 5'-CTTAAGCCTAGTGACTGTATTACCCTGACTCAGGTATCCCCA CTTTCCCCACGCTAGGTCCAGCCATGGAGTATCCCTATGACGTCCCGGACTATGCAGGATCCTATCCATATGACGTT CAGATTACGCTGAGCTGCGCTCGGAGCTGCCAGCGTGCCCGGTGCGGCGACAGCAGCAGCGACAGCGACGGGAC CACCC-3', with crRNA sequence underlined and *Dmrt2* ATG initiation codon in bold) into the pronucleus of B6D2F2 zygotes. Viable two-cell stage embryos were transferred to pseudopregnant CD1 females. Founder mice with the modified *Dmrt2*^{2xHA} allele were screened for appropriate integration of the transgenic sequences at the knock-in region as well as for the presence of predicted (<http://crispr.dbcls.jp/>) potential off-targets followed by PCR followed by Sanger sequencing of the PCR products (Genewiz). They were then crossed with C57BL/6J. Germline transmission of the selected *Dmrt2*^{2xHA} founder mouse was then validated by PCR. Selected founders were then maintained in this background during at least three generations before to be used in this study.

The *Dmrt2* null and WT alleles were detected by PCR using primers Fwd: 5'-CGAATCTTTCGGACACTGTAGA-3'; Rev WT: 5'-CCAGAC CCTCAAGCACTCAA-3'; Rev KO: 5'-AGCGCTCCCCTACCCGGTA-3'. The *Dmrt2*^{Tg} allele was detected by PCR using primers Fwd Rosa26 5'-AAACTGGCCCTTGCCATTGG-3'; Fwd eGFP 5'-AACGAGAAGCGCG ATCACAT-3'; Rev Rosa26 5'-GTCTTTAATCTACC TCGATGG-3'. The *Pax6*^{sey} mutated allele was detected by high-resolution DNA melting analysis (HRMA; Reed et al., 2007) using primers 5'-AGGGGAGAGAACACCAACT-3' and 5'-CATCTGAGCTTCATCCGAGTC-3'. The *Dmrt2*^{2xHA} allele was detected by PCR using primers inside the inserted 2XHA sequence (5'-TATCCCTATGACGTCCCGGAC-3' and 5'-AGCGTAATCTGGAACGTCATAT-3') and flanking the inserted 2XHA sequence (5'-TTCCAGTTCGTTTCCCCAGCA-3' and 5'-GTACTTCTCCGCTGCCCTCAA-3'). As previous studies did not reveal any differences in *Dmrt2* nor *Pax6* gene expression between sexes, nonsex-determined embryos have been used in all our analyses.

Immunofluorescence and in situ hybridization. For immunofluorescence (IF), dissected brains of embryos (E12.5) were fixed for 2 h at 4°C in 4% paraformaldehyde (PFA)/phosphate-buffered saline (PBS). Tissues were then rinsed with ice-cold PBS and

cryopreserved by overnight (O/N) incubation in 30% sucrose/PBS O/N, subsequently embedded in gelatin (7.5% gelatin, 15% sucrose/PBS), and sectioned in 14 μm cryostat sections. Sections were then rinsed in PBS, permeabilized, and blocked in a solution of PBS with 0.3% Triton X-100 containing 10% goat serum for at least 2 h at RT and then incubated with primary antibodies diluted in blocking serum O/N, at 4°C. Slides were incubated in secondary antibodies diluted in PBST for 2 h at RT. The following primary antibodies were used: rabbit anti-Dmrt2 (1:1,000; De Clercq et al., 2018), rabbit anti-Flag (1:500, Sigma, catalog #F3165), rabbit anti-HA (1:500, Abcam, catalog #ab9110), and mouse anti-Zfp423 (1:500, Santa Cruz Biotechnology, catalog #sc-393904). The following secondary antibodies were used: anti-mouse Alexa Fluor 488 (1:400, Invitrogen, catalog #A-11017), anti-rabbit Alexa Fluor 488 (1:400, Invitrogen, catalog #A-11008), anti-mouse Alexa Fluor 594 (1:400, Invitrogen, catalog #A-11005), and anti-rabbit Alexa Fluor 594 (1:400, Invitrogen, catalog #A-11012). Sections were counterstained with DAPI. Images were acquired with a Carl Zeiss LSM 710 confocal microscope using Zen-Black software or Nikon A1R gallium arsenide phosphide inverted confocal microscope and processed using ImageJ and Photoshop software.

In situ hybridization (ISH) on whole brains or sections were processed with digoxigenin (Dig)-labeled riboprobes as described (Schaeren-Wiemers and Gerfin-Moser, 1993; Wilkinson and Nieto, 1993). The brains of embryos (E11.5, E12.5, and E15.5) and newborn mice (P7) were fixed in 4% PFA/PBS at 4°C, O/N. For ISH on sections, the brains were infused in 30% sucrose/PBS, O/N, and frozen in gelatin (7.5% gelatin, 15% sucrose/PBS). Then, 20 μm cryostat sections were collected. For ISH on whole mount, the brains were dehydrated by rinsing 15 min (min) in successive baths of MetOH-PTw (25, 50, 75, and 100%) and stored at -20°C . The probes were generated from the following previously described cDNA clones: *Dmrt2* (Saulnier et al., 2013), *Gsx1* and *Gsx2* (Toresson et al., 2000), *Pax6* (Hamasaki et al., 2004), *Rorb* (De Clercq et al., 2018), *Wnt3a* (Monuki et al., 2001), *Wnt8b* (Lee et al., 2000), and *Zfp423* (Masserdotti et al., 2010). Images were acquired with an Olympus SZX16 stereomicroscope and an XC50 camera, using the Imaging software cellSens.

Quantification of the dorsal surface area of the cortical hemisphere of E18.5 embryos was obtained by taking measurements from images of whole brains. The surface areas of the primary motor, sensorimotor, and visual neocortex in P7 brains were measured by taking measurements from the images and outlining the corresponding regions with specific probes as indicated in the text. The results are presented as the ratio of the M1, S1, and V1 areas relative to the total dorsal surface area of the cortex. Micrographs were taken with an Olympus SZX16 stereomicroscope. Measurements were done using the Imaging software cellSens. All quantified data are expressed as mean values \pm standard deviation (SD). Significance tests were performed using a two-tailed Student's *t* test; *p* values <0.05 were regarded as statistically significant. Each experiment was repeated on at least four biological samples for each genotype.

Whole-mount X-gal staining of embryos. Embryos were fixed in 4% PFA for 1 h at RT and rinsed in detergent solution (2 mM MgCl_2 , 0.01% sodium deoxycholate, 0.02% NP-40 diluted in 0.1 M, pH 7.3, phosphate buffer). Embryos were then incubated at 37°C in a staining solution composed of detergent solution with 5 mM $\text{K}_3\text{Fe}(\text{CN})_6$, 5 mM $\text{K}_4\text{Fe}(\text{CN})_6$, and 1 mg/ml of X-gal. Before clearing embryos were progressively dehydrated in increasing concentrations of MetOH. After several washes in 100% MetOH, embryos were incubated in a solution of MetOH:BABB (1:1) before being incubated and stored in 100% BABB. BABB is made of one part benzyl alcohol for two parts of benzyl benzoate.

RNA isolation and RT-qPCR. The cortex of embryos was dissected in RNAase-free cold $1\times$ PBS and then immediately frozen at -80°C . RNA extraction was performed using the Monarch Total RNA Miniprep Kit (New England Biolabs, catalog #T2010s) according to the manufacturer's protocol. cDNA was synthesized starting from 1–2 μg of total RNA using the iScript cDNA Synthesis Kit (Bio-Rad, catalog #1708891). RT-qPCRs were carried out with the Luna Universal qPCR Master Mix (New England Biolabs, catalog #M3003) using the StepOne Plus Real-Time PCR system (Applied Biosystems). RT-qPCRs primers used were as follows: *Pax6* (5'-AGGGCAATCGGAGGGAGTAA-3' and 5'-CAGGTTGC GAAGAACTCTGTTT-3'); *Emx2* (5'-GTCCACCTTCTACCCCTGG-3' and 5'-CCACCACGTAATGGTTCTTCTC-3'); *Lhx2* (5'-TGGCAGCATCTACTGCAAAG-3' and 5'-TGTGCATGTGAAGCAGTTGA-3'); *Wnt3a* (5'-CAGGAACTACGTGGAGATC ATGC-3' and 5'-CATGGACAAAGGCTGACTCC-3'); *Wnt8b* (5'-CAGCTCTGCTGGGGTTATGT-3' and 5'-CTGCTTGGAAATTGCCTCTC-3') and *GAPDH* (5'-GTGAAGGTCGGTGTGAACG-3' and 5'-AGGGGTCGTTGATGGCAACA-3') used as a reference gene for normalizing gene expression results. Error bars show the standard deviations of at least three independent experiments. To detect by RT-PCR the *Dmrt2* tagged allele in dissected cortices of *Dmrt2*^{2xHA} transgenics, primers 5'-TTCCAGTTTCGTTTCCCAGCA-3' and 5'-GTACTTCTCGCTGCCCTCAA-3' were used.

Plasmids. For reporter assays, to generate the pGL4.23-*E60*- tk-luc reporter plasmid, a 2,350 bp fragment containing the *Pax6 E60* enhancer was amplified by PCR from the *E60* hsp68-LacZ-pA construct (McBride et al., 2011) using primers 5'-TGGCCTAACTGGCCGGTACCTGCAATGCTAGGGATCAAACC-3' and 5'-TCCTCGAGGCTAGCGAGCTCATCTTGCC GGTCACCTCACTA-3' and cloned into the NotI and SpeI restriction sites of the pGL4.23-based luciferase reporter plasmid containing a 32 bp thymidine kinase (tk) minimal promoter. The pGL4.23-Gsx1enh-tk-luc reporter was generated by amplifying by PCR a genomic fragment with primers 5'-TGCAATGCTAGG GATCAAACC-3' and 5'-TCCTCGAGGCTAGC GAGCTCTTGCCGGTACCTCA CTA-3' from a Bac-Pac containing the *Gsx1* locus (CHORI, RP24-245J15) and cloning it into the KpnI and SacI sites of the pGL4.23 vector. The 5XUAS-tk-luc reporter plasmid contains five GAL4 binding sites inserted upstream of a herpes simplex virus (HSV) thymidine kinase (tk) promoter driving the expression of the firefly luciferase. The mouse *Pax6* expression plasmid was generated by amplifying by PCR the *Pax6* ORF from a pEFX-Pax6 expression vector (obtained from E.A. Grove) using primers 5'-AAGAGGACTTGAATTCGCAGAACAGTCACAGC

GGAGTG-3' and 5'-GTTCTAGAGGCTCCAGTTACTGTAATCGAGGCCAGTAC-3' containing EcoRI and XhoI and cloning it into the corresponding sites of a pCS2-Myc expression vector. The pCS2-Flag-*mDmrta2* has been generated by cloning the *mDmrta2* ORF into the EcoRI and XhoI sites of the pCS2-Flag vector. The pCS2 Flag *mDmrta2*ΔDM with the DM domain deleted contains amino acids 1–62 and 125–531 of WT *mDmrta2*. The *mDmrta2* C-R mutant was generated by amplifying two fragments encoding the N-terminal and C-terminal region of *Dmrta2* using primers 5'-CATTCTGCC TGGGGACGTCGGAGC-3' and 5'-CTTCTCCGCTGCCCTCAACAGCAG-3' for the N-terminal region, and primers 5'-GC GCGCGAGTTGCAATTGCT-3' and 5'-CCGGGCCCAATGCATTGGCG-3' for the C-terminal region, and assembling them with a third overlapping fragment generated in vitro (IDT, gBlocks Gene Fragment) encoding the *Dmrta2* DM domain in which an arginine replaces each cysteine, and cloning them into the HindIII and NotI sites of the pCS2-Flag vector using the Gibson Assembly Cloning Kit (New England Biolabs, catalog #E5510S). The pCDNA3-Myc-*Zfp423* expression plasmid was described previously (Masserdotti et al., 2010). The pCMV-Gal4-*Dmrta2*(FL) and pCMV Gal4-*Dmrta2* (126–531) fusion constructs have been generated by amplifying by PCR and cloning the corresponding *Dmrta2* fragments in frame with the Gal4 DBD into the BamHI site of the pCMV-Gal4 vector (Nan et al., 1997).

For coimmunoprecipitation, the *mDmrta2* aDM mutant has been generated by PCR amplifying two overlapping fragments encoding the N-terminal and C-terminal region of *Dmrta2* using primers 5'-CATTCTGCCTGGGGACGTCGGAGC-3' and 5'-CGTACAGCAATTGCAACTCGCGCGCTTCTCCGCTGCCCTCAACAGC-3' for the N-terminal region and primers 5'-GC GCGCGAGTTGCAATTGCT-3' and 5'-CCGGGCCCAATGCATTGGCG-3' for the C-terminal region and cloning them into the HindIII and NotI sites of the pCS2-Flag vector using the Gibson Assembly Cloning Kit (New England Biolabs, catalog #E5510S).

For GST pull-down assays, cDNAs encoding *mDmrta2* and a deletion mutant containing only the DM domain (GST-*Dmrta2* DM, containing aa 42–133) and *mDmrta3* were inserted in pGEX plasmids.

Cell culture. Embryonal carcinoma P19 cells and human embryonic kidney 293T (HEK293T) were grown in D-MEM medium (Invitrogen, catalog #61965-059) supplemented with 10% fetal bovine serum (Invitrogen, catalog #26140079) and 100 U/ml penicillin-streptomycin (Invitrogen, catalog #15140-122) and maintained in culture flasks at 37°C under 5% CO₂. The cells were subcultured when they reached 80% confluency.

Luciferase reporter assays. Reporter assays using the *Pax6 E60* enhancer tk-luc reporter plasmid (*Pax6 E60*-tk-luc) have been performed in P19 cells. Cells were plated in 12-well plates and after 24 h, transfected using the CalPhos Mammalian Transfection Kit (Takara, catalog #631312) with 500 ng of the *Pax6*-E60-tk-luc luciferase reporter, or an “empty” tk-luc reporter vector, with or without pCS2-Flag-*mDmrta2* and pCDNA3-Myc-*Zfp423* expression plasmids, together with a plasmid encoding the *Renilla* luciferase gene. After 48 h, cells were washed with 1 × PBS, total cellular extracts were prepared, and luciferase activity was measured using the Dual-luciferase Reporter Assay System (Promega, catalog #E1960). Ratios of *luc*/*Renilla* luminescence were calculated and presented as fold activation for each reporter. The HDAC class I inhibitor Romidepsin (MedChemExpress, catalog #HY-15149) was used at 0.005–0.01 μM. It was added 24 h after transfection and 24 h before performing the luciferase reporter assays. At least three independent transfections have been performed for each experiment. Each dot represents the mean value obtained from one transfection performed in triplicate.

Reporter assays using the 5XUAS-tk-luc reporter have been performed in HEK293T cells. HEK293T cells (2.5 × 10⁵ cells per well) were cultured and transiently transfected as described for P19 cells with 200 ng of 5XUAS-tk-luc reporter construct, with or without pCMV-Gal4-*Dmrta2*, pCMV-Gal4-*Dmrta2*(126–531), and/or pCDNA3-Myc-*Zfp423* expression plasmids. To maintain the same amount of transfected DNA and to avoid squelching artifacts, the different amounts of cotransfected plasmid were complemented in equimolar manner by using the corresponding empty plasmid. Forty-eight hours posttransfection, cells were lysed, and luciferase activities were measured using the Single Glo luciferase reporter assay (Promega). Results were normalized for transfection efficiency using total protein content.

GST pull-down. pCDNA3-Myc-*Zfp423* plasmid has been transcribed and translated using in vitro T7-coupled reticulocyte lysate. GST fusion proteins were incubated with labeled proteins in 200 μl binding buffer (Tris 20 mM, pH 7.4, NaCl 0.1 M, EDTA 1 mM, glycerol 10%, Igepal 0.25% with 1 mM DTT, and 1% milk) for 2 h at RT. After washing, bound proteins were separated by SDS-PAGE and visualized by Western blot.

Coimmunoprecipitation and western blot. For coimmunoprecipitation (Co-IP), transfected HEK293T cells were lysed in IPH buffer (20 mM Tris-HCl, pH 7.5, 150 mM NaCl, 2 mM EDTA, 1% NP-40) supplemented with protease inhibitor cocktail (Roche, cOmplete EDTA-free Protease Inhibitor Cocktail, catalog #05892791001) and incubated for 15 min, at 4°C. Cell lysates were then centrifuged twice at 13,000 rpm for 30 min, at 4°C to remove debris. Part of the lysate (2.5%) was kept as a positive input control. Co-IPs were performed by incubating cell lysates (1 mg) with 5 μl of the indicated antibodies at 4°C with rotation, O/N. Then, 20 μl of magnetic beads G (Cell Signaling, catalog #9006s) was then added for 4 h, at 4°C. After four washes with IPH buffer, bound protein complexes were eluted by incubating beads in Laemmli sample buffer for 10 min, at 90°C. Immunoprecipitated protein complexes were subjected to Western blot analysis as described below.

For Western blot analysis, protein extracts from dissected cortices were prepared in RIPA buffer (50 mM Tris-HCl, pH 8, 150 mM NaCl, 1% NP-40, 0.5% sodium deoxycholate, 0.1% SDS), and those from cultured cells were prepared in IPH buffer supplemented with protease inhibitor cocktail. Homogenates were quantified by using the Bradford Assay (OD 595 nm) and centrifuged for 15 min, at 10,000 × *g*, at 4°C, and the supernatants were collected. Equal quantities of protein

(60 µg/lane) were separated by 8–10% SDS-PAGE in a chamber filled with running buffer (0.1% SDS, 25 mM Tris base, 190 mM glycine; adjust pH to 8.3) and placed into a transfer cassette with transfer buffer (25 mM Tris-base, 190 mM glycine, 20% MetOH, adjust pH to 8.3), and the proteins were transferred onto a polyvinylidene difluoride (PVDF, Cytiva, catalog #10600029) membrane. Then the membrane was blocked with Tris-buffered saline (TBS) with 5% non-fat milk for 1 h, at RT, and incubated at 4°C, O/N, with the following primary antibodies: rabbit anti-Flag (1:1,000); rabbit anti-HA (1:1,000); rabbit anti-H3 (1:50,000, Millipore, catalog #07-690); mouse anti-Myc (1:1,000, Sigma, catalog #M4439); mouse anti-Zfp423 (1:1,000); and the NurD complex antibody kit (Cell Signaling, catalog #8349T). Following rinsing three times with TBS/Tween 20, the membranes were incubated with the following secondary antibodies: anti-mouse IgG HRP (1:5,000, Jackson ImmunoResearch, catalog #115-035-062) and anti-rabbit IgG HRP (1:3,000, Cell Signaling, catalog #7074) for 1 h, at RT. Protein levels were normalized to H3, and all proteins were detected using the Novex ECL Chemiluminescent Substrate Reagent Kit (Invitrogen, catalog #WP20005).

Electrophoretic mobility shift assays. Electrophoretic mobility shift assays (EMSA) were performed using nuclear extracts prepared from HEK293T cells transfected with expression vectors of either DMRTA2 or DMRTA2^{R116P} as described (Dignam et al., 1983). Total protein concentrations were determined by Bradford assays (Bio-Rad). DMRTA2 WT and DMRTA2^{R116P} proteins were also produced using the Transcription and Translation (TnT) system (Promega). EMSAs were performed as described previously (Van Lint et al., 1994). Briefly, 2 µl of TNT preparation or 1 µg nuclear extracts from HEK293T cells either nontransfected or transfected with DMRTA2 WT or DMRTA2 mutated were first incubated for 10 min in the absence of a probe in a reaction mixture containing 10 µg of DNase-free BSA (Bioké), 2 µg of poly(dI-dC) (Sigma) as nonspecific competitor DNA, 50 µM ZnCl₂, 0.25 mM DTT, 20 mM HEPES, pH 7.3, 60 mM KCl, 1 mM MgCl₂, 0.1 mM EDTA, and 10% (v/v) glycerol. A total of 30,000 cpm of probe (10–40 fmol) was then added to the mixture that was incubated for 20 min. Samples were subjected to electrophoresis at room temperature on 6% polyacrylamide gels at 120 V for 2–3 h in 1× TGE buffer (25 mM Tris-acetate, pH 8.3, 190 mM glycine, and 1 mM EDTA). Gels were dried and autoradiographed for 48–72 h at –80°C. The probe used are oligonucleotides 5RE described in Murphy et al. (2007).

Rapid immunoprecipitation mass spectrometry of endogenous protein. Rapid immunoprecipitation mass spectrometry of endogenous protein (RIME) experiments were carried out as previously described (Mohammed et al., 2016) with minor modifications. Briefly, E12.5 cortices were dissected on ice in RNAase-free ice-cold 1× PBS and fixed for 15 min in 1% formaldehyde (Thermo Scientific, catalog #28906) in 1× PBS at RT. The cross-linking was quenched by adding glycine to a final concentration of 125 mM and incubating samples for 8 min. Subsequently, the fixed tissues were pelleted and washed in ice-cold PBS. Nuclear extraction was done using ice-cold LB1 buffer [50 mM HEPES-KOH, pH 7.5, 140 mM NaCl, 1 mM EDTA, 10% glycerol, 0.5% NP-40 (vol/vol) and 0.25% Triton X-100 (vol/vol)], incubating cells on rotation for 10 min at 4°C. The suspension was then centrifuged at 2,000 × g for 5 min at 4°C and the obtained nuclear pellet was washed in ice-cold LB2 buffer (10 mM Tris-HCl, pH 8.0, 200 mM NaCl, 1 mM EDTA, 0.5 mM EGTA). Pelleted nuclei were subsequently resuspended in LB3 buffer [10 mM Tris-HCl, pH 8.0, 100 mM NaCl, 1 mM EDTA, 0.5 mM EGTA, 0.1% sodium deoxycholate (wt/vol) and 0.5% N-lauroylsarcosine (wt/vol)] and, after an incubation of 15 min, were subjected to three cycles of sonication (30 s ON/30 s OFF for 10 min, at 200 W, high setting, Bioruptor, Diagenode). Triton X-100 was added to the sonicated lysate to a final concentration of 1%. The obtained chromatin was then cleared by centrifugation at 20,000 × g for 10 min, at 4°C, and the supernatant was collected. All lysis buffers were supplemented with protease inhibitors before use.

Antibody-bound beads were generated by incubating 100 µl of Protein G magnetic beads (Cell Signaling, catalog #9906) with 5 µl rabbit anti-HA (Abcam, catalog #ab9110) or rabbit anti-IgG (Merck, catalog #12-370) in PBS/BSA and incubated in rotation at 4°C, O/N. The next day, the antibody-bound beads were washed three times in PBS/BSA to remove any unbound antibodies. For immunoprecipitation, 2 mg of protein lysate was incubated O/N, with 100 µl antibody-bound beads at 4°C. The next day, the bead-bound complexes were washed nine times in RIPA buffer (50 mM HEPES, pH 7.6, 1 mM EDTA, 0.7% sodium deoxycholate, 1% NP-40, and 0.5 M LiCl) at 4°C and then washed two times with a cold 100 mM ammonium hydrogen carbonate (AMBC) solution. Finally, the beads were transferred to new tubes, snap-frozen at –80°C, and stored at this temperature until mass spectrometry analysis.

Mass spectrometry. The samples were treated using filter-aided sample preparation (FASP). To first wash the filter, 100 µl of 1% formic acid was placed in each Millipore Microcon 30 MRCFOR030 Ultracel PL-30, and samples were centrifuged for 15 min, at 14,500 rpm. For protein adjustment, 40 µg of protein in 150 µl of 8 M urea buffer (urea 8 M in 0.1 M Tris, pH 8.5) was placed individually in a column and centrifuged for 15 min, at 14,500 rpm. The filtrate was discarded, and the columns were washed three times with 200 µl of urea buffer followed by centrifugation for 15 min, at 14,500 rpm. For the reduction step, 100 µl of dithiothreitol (DTT) was added and mixed for 1 min, at 400 rpm with a thermomixer; incubated for 15 min, at 24°C; and centrifuged for 15 min, at 14,500 rpm. The filtrate was discarded and 100 µl of urea buffer was added before another centrifugation for 15 min, at 14,500 rpm. An alkylation step was performed by adding 100 µl of iodoacetamide (IAA), in urea buffer in the column, mixing for 1 min, at 400 rpm, incubating for 20 min in the dark, and centrifuging for 10 min, at 14,500 rpm. To remove the excess IAA, 100 µl of urea buffer was added and the samples were centrifuged for 15 min, at 14,500 rpm. To quench the remaining IAA, 100 µl of DTT was added to the column; mixed for 1 min, at 400 rpm; incubated for 15 min, at 24°C; and centrifuged for 10 min, at 14,500 rpm. Excess DTT was removed by adding 100 µl of urea buffer and centrifuging for 15 min, at 14,500 rpm. The filtrate was discarded, and the column was washed

three times with 100 μ l of sodium bicarbonate buffer 50 mM (ABC) followed by centrifugation for 10 min, at 14,500 rpm. The last 100 μ l were kept at the bottom of the column to avoid any evaporation in the column. For digestion, 80 μ l of mass spectrometry grade trypsin (1/50 in ABC buffer) was added to the column; mixed for 1 min, at 400 rpm; and incubated at 24°C, O/N in a water-saturated environment. The Microcon columns were placed on a LoBind tube of 1.5 ml and centrifuged for 10 min, at 14,500 rpm. Then, 40 μ l of ABC buffer was added to the column before centrifugation for 10 min, at 14,500 rpm. Then, 10% trifluoroacetic acid (TFA) was added to the content of the LoBind tube to obtain 0.2% TFA. The samples were dried in a SpeedVac up to 20 μ l and transferred for injection.

The samples were analyzed using nano-LC-ESI-MS/MS (timsTOF Pro, Bruker) coupled with a UHPLC nanoElute (Bruker). Liquid chromatography was separated at 50°C and at a flow rate of 200 nl/min by nanoUHPLC (nanoElute, Bruker) on a C18 column (25 cm \times 75 μ m ID) with integrated CaptiveSpray insert (Aurora, IonOpticks). Mobile phases A and B were water with 0.1% formic acid (v/v) and ACN with formic acid 0.1% (v/v), respectively. Samples were loaded directly on the analytical column at a constant pressure of 800 bar. The digest (1 μ l) was injected, and the organic content of the mobile phase was increased linearly from 2 to 15% B within 40 min, followed by an increase to 25% B within 15 min, and further to 37% B in 10 min, followed by a washing step at to 95% B in 5 min. Data acquisition on the timsTOF Pro was performed using Hystar 6.1 and tims Control 2.0. The timsTOF Pro data were acquired using 160 ms TIMS accumulation time, and mobility coefficients (1/K0) range from 0.75 to 1.42 Vs/cm². Mass spectrometry analysis was carried out using the parallel accumulation-serial fragmentation (PASEF; Meier et al., 2018) acquisition method. One MS spectra followed by PASEF MSMS spectra per total cycle of 1.16 s. All MS/MS samples were analyzed using Mascot (Matrix Science; version 2.8.1). Scaffold (version Scaffold_5.0.0, Proteome Software) was used to validate MS/MS-based peptide and protein identifications. The mass spectrometry proteomics data have been deposited to the ProteomeXchange Consortium via the PRIDE (Perez-Riverol et al., 2025) partner repository with the dataset identifier PXD062221 and 10.6019/PXD062221.

Human subjects and clinical evaluation. As a result from a GeneMatcher match (Sobreira et al., 2015), we studied a Pakistani consanguineous family with three affected individuals, V-3, V-5, and V-7 (Fig. 6A,C). The clinical evaluation of the probands was performed at the Aga Khan University Hospital, Karachi. Detailed clinical evaluation was carried out in two affected persons, V-3 and V-5 (Extended Data Table 6-1); however, the affected person V-7 showed similar clinical features. This study was conducted with ethical approval from the Aga Khan University Hospital, Karachi. We obtained written informed consent, and blood samples were taken from all the available persons (III-7, IV-1, IV-5, IV-7, V-3, V-5, V-7) in the family. Genomic DNA was extracted as described previously (Sambrook and Russell, 2006). The MRI of V-3 (6 years) was performed, which revealed microcephaly, a simplified gyral pattern along with agenesis of the corpus callosum and colpocephaly. Electroencephalography (EEG) was performed on the affected person, V-5 (5 years).

Whole-exome sequencing. We performed whole-exome sequencing (WES) using DNA samples of two affected individuals, V-3 and V-5 (Fig. 6A,C). WES and further data analysis to find the exact causative variant has been performed as described (Yousaf et al., 2022, 2023). The combined analysis of WES data of V-3 and V-5 revealed three shared homozygous variants: *C1orf109*: NM_001303030.2: c.373C>A:p.(Leu125Ile), *DMRTA2*: NM_032110.3: c.347G>C:p.(Arg116Pro), and *TMEM161A*: NM_001256766.3: c.745G>A:p.(Ala249Thr) between both the WES-analyzed persons. We further excluded two variants located in *C1orf109* and *TMEM161A* genes, as the variant in *C1orf109* was found 11 \times in homozygous state in the gnomAD database (v4.1.0), and the *TMEM161A* variant did not segregate with the phenotype. *DMRTA2*: p.(Arg116Pro) is the only homozygous variant that segregated (tested by Sanger sequencing) with the phenotype in this consanguineous family (Fig. 6). The variant p.(Arg116Pro) has a Combined Annotation Dependent Depletion (CADD) score (v1.6) of 31 (Kircher et al., 2014) and is predicted as “deleterious” by multiple in silico-prediction programs and classified as a variant of uncertain significance, according to the ACMG classification criteria PM2, PP1, PP3, and PP4 (Richards et al., 2015).

Statistical analysis. Statistical significance was determined by the Student's *t* test or the one-way analysis of variance (ANOVA), with a threshold for significance set to $p < 0.05$. All results are plotted as the mean \pm SD, as indicated in the figure legends.

Results

***Dmrta2* cooperates with *Pax6* in defining telencephalic dorsoventral compartments and acts through its repression to control cortical patterning**

To test the hypothesis that *Dmrta2* acts through *Pax6* to control cortex development, we generated double mutants by intercrossing *Dmrta2*^{+/-} mice with *Pax6*^{sey/+} mice which have a point mutation in the *Pax6* gene creating a null allele (Hill et al., 1991). Embryos were collected at three embryonic time points (E11.5, E15.5, and E18.5) to measure the surface area of their hemispheres. We found that the cerebral hemispheres of *Pax6*^{sey/sey} embryos and *Dmrta2*^{-/-} embryos were smaller compared with embryos at E18.5, with the reduction in *Dmrta2*^{-/-} being more severe (-60.1% \pm 2.5% in *Dmrta2*^{-/-} compared with -16.9% \pm 7.2% in *Pax6*^{sey/sey}) and detected at an earlier stage in *Dmrta2*^{-/-} embryos than in *Pax6*^{sey/sey} embryos. In the *Dmrta2*^{-/-}; *Pax6*^{sey/sey} embryos, the cerebral hemispheres were virtually absent. Notably, the extent of the reduction in *Dmrta2*^{-/-} embryos was less severe in the absence of one allele of *Pax6* (-31.6% \pm 6.5% in *Dmrta2*^{-/-}; *Pax6*^{sey/+} compared with -60.1% \pm 2.5% in *Dmrta2*^{-/-}; Fig. 1A). This rescue was already visible at earlier stages: at

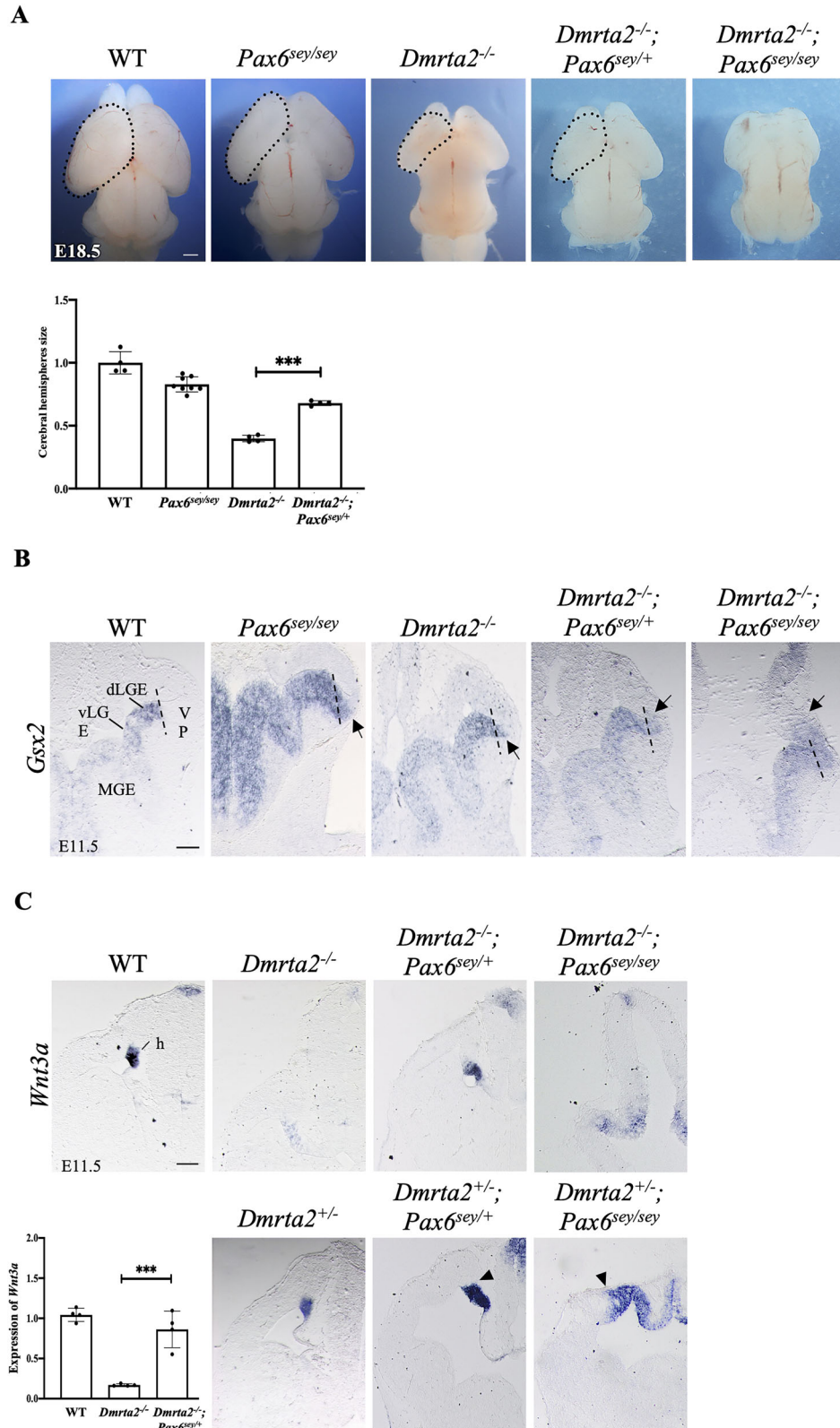


Figure 1. Cortical phenotype of *Dmrta2*^{-/-} embryos in the absence of one or two Pax6 alleles. **A**, Dorsal views of the brain of E18.5 embryos of the indicated genotypes. Scale bar, 100 μ m. Graphs representing the measured surface area of the cerebral hemispheres of *Pax6*^{sey/sey}, *Dmrta2*^{-/-} and *Dmrta2*^{-/-}; *Pax6*^{sey/+} compared with WT set to 1 are shown. ****p* < 0.001, Student's *t* test. Note that the reduction in cerebral hemisphere size observed in *Dmrta2*^{-/-} embryos is less severe in the absence of a Pax6 allele. An analysis of the size of the cerebral hemispheres in these embryos collected at E11.5 and E15.5 embryos is presented in Extended Data Figure 1-1. **B**, Coronal sections through the brain of E11.5 embryos of the indicated genotypes processed by ISH for Gsx2. Note that Gsx2 expression in the telencephalon only slightly crosses the pallium-subpallium (PSB) boundary in *Pax6*^{sey/sey},

E11.5 ($-38.6\% \pm 5.6\%$ in $Dmrta2^{-/-}; Pax6^{sey/+}$ compared with $-48.2\% \pm 6.4\%$ in $Dmrta2^{-/-}$) and E15.5 ($-34.5\% \pm 4.2\%$ in $Dmrta2^{-/-}; Pax6^{sey/+}$ compared with $-48.9\% \pm 7.7\%$ in $Dmrta2^{-/-}$; Extended Data Fig. 1-1). Analysis by in situ hybridization of the expression of the subpallial marker *Gsx2* expressed at a high level in progenitors of the dorsal LGE (dLGE) revealed that its expression in the single KO embryos and in $Dmrta2^{-/-}; Pax6^{sey/+}$ mutants remained confined to the subpallium or only very slightly crossed the pallium-subpallium boundary (PSB) while it distinctly extended into the abortive cortical primordium of the double KO embryos (Fig. 1B). Similarly, *Gsx1* that is also bound by *Dmrta2* (Konno et al., 2019) and is expressed mainly in MGE and vLGE (Pei et al., 2011) remains restricted to the ventral telencephalon in $Pax6^{sey/sey}$, $Dmrta2^{-/-}$, and $Dmrta2^{-/-}; Pax6^{sey/+}$ embryos but appears to expand into the reduced telencephalon of $Dmrta2^{-/-}; Pax6^{sey/sey}$ embryos (Extended Data Fig. 1-2). These data provide additional evidence for the importance of a correct balance between *Dmrta2* and *Pax6* for normal cortical hemisphere growth. They also reveal that *Dmrta2* and *Pax6* cooperate in maintaining cortical identity in dorsal telencephalic progenitors.

Pax6 suppresses medial cortical fate in the cortical neuroepithelium (Godbole et al., 2017). Therefore, and because *Pax6* is excluded from the hem (Saulnier et al., 2013; De Clercq et al., 2018), we hypothesized that the medial expansion of *Pax6* observed upon the loss of *Dmrta2* could be responsible for the suppression of hem formation. To test this hypothesis, we examined by in situ hybridization the expression of *Wnt3a* which identifies the cortical hem, and *Wnt8b*, which marks the dorsomedial telencephalic primordium and eminentia thalami, both being upregulated in the absence of *Pax6* (Godbole et al., 2017), in the cortex of E11.5 homozygous and heterozygous *Dmrta2* mutants with the loss of one *Pax6* allele.

As previously reported (Saulnier et al., 2013), in the medial telencephalon of $Dmrta2^{-/-}$ embryos, *Wnt3a* is strongly reduced. As shown in Figure 1C, *Wnt3a* is much less affected in $Dmrta2^{-/-}; Pax6^{sey/+}$ embryos than in $Dmrta2^{-/-}$ embryos. RT-qPCR on RNA extracted from telencephalic tissue isolated from E11.5 embryos confirmed the drastic downregulation of *Wnt3a* in $Dmrta2^{-/-}$ embryos and that a rescue of its expression occurs upon the loss of one *Pax6* allele. While compared with controls *Wnt3a* is slightly reduced in intensity in $Dmrta2^{+/-}$ embryos, its expression domain is expanded in $Dmrta2^{+/-}; Pax6^{sey/+}$ embryos and even more in $Dmrta2^{+/-}; Pax6^{sey/sey}$ embryos. Such an expansion is however not visible anymore in the abortive cortex of the $Dmrta2^{-/-}; Pax6^{sey/sey}$ embryos.

As reported previously, in the medial telencephalon of $Dmrta2^{-/-}$ embryos, *Wnt8b* is downregulated in the telencephalon but not in the eminentia thalami (Saulnier et al., 2013). In $Dmrta2^{+/-}$ embryos, such a phenotype is not observed and *Wnt8b* appears similar to controls. In $Dmrta2^{+/-}; Pax6^{sey/+}$ embryos, *Wnt8b* expression domain appears however to extend more into the lateral part of the telencephalon ($1.2 X \pm 0.06$, measuring *Wnt8b* expression domain from the ventral extent of the telencephalon) than in $Dmrta2^{+/-}$ embryos. The hem region itself as suggested by the more intense *Wnt8b* expression appears also extended in these $Dmrta2^{+/-}; Pax6^{sey/+}$ embryos, and even more in $Dmrta2^{+/-}; Pax6^{sey/sey}$ embryos, as observed for *Wnt3a* (Extended Data Fig. 1-3). Thus, mediolateral patterning of the cerebral cortex and cortical hem formation is regulated by *Dmrta2* through repression of *Pax6*.

Pax6 promotes rostral area identity in the developing neocortex (Bishop et al., 2000, 2002; O'Leary and Sahara, 2008). *Pax6* is reduced in the cortex of transgenic mice conditionally overexpressing *Dmrta2* that have expanded V1 area (De Clercq et al., 2018). It could therefore be that it is the decreased level of *Pax6* that caudalizes the neocortex of mice expressing in excess *Dmrta2*. Therefore, we generated transgenic mice conditionally overexpressing both *Dmrta2* and *Pax6* by crossing $Emx1^{Cre}; Dmrta2^{Tg/+}$ (De Clercq et al., 2018) with $Emx1^{Cre}; Pax6^{Tg/+}$ mice (Berger et al., 2007). We examined area formation at P7 in the cortex of heterozygous double transgenics ($Emx1^{Cre}; Dmrta2^{Tg/+}; Pax6^{Tg/+}$) and single transgenic mice ($Emx1^{Cre}; Dmrta2^{Tg/+}$ and $Emx1^{Cre}; Pax6^{Tg/+}$), as homozygous ones exhibit early lethality, possibly due to sustained expression of *Dmrta2* and *Pax6* in postmitotic cortical cells. This analysis was carried out by whole-mount in situ hybridization monitoring *Rorb* expression, which demarcates the S1, A1, and V1 area, measuring the size of the V1 area relative to the total hemisphere size (Fig. 2). We found that the V1 area that are expanded in *Dmrta2* overexpressing mice are reduced when *Pax6* is also overexpressed, as observed in *Pax6* overexpressing mice. These findings support the hypothesis that *Dmrta2* controls cortical arealization by regulating the level of *Pax6* expression.

***Dmrta2* can act as a DNA-binding repressor on the *Pax6* E60 enhancer and a point mutation in its DM domain causes microcephaly in human**

Pax6 has been shown to be deregulated by the loss or gain of function of *Dmrta2* in the developing cortex (Konno et al., 2012; Saulnier et al., 2013). The deregulation of *Pax6* is rapid as it is already observed at E12.5 in $Nestin^{Cre}; Dmrta2^{fl/fl}$ mice (De Clercq et al., 2018). It can be seen already at E9.5 in *Dmrta2* null mutants before the disruption of Wnt signaling that can

$Dmrta2^{-/-}$ and $Dmrta2^{-/-}; Pax6^{sey/+}$ embryos, and robustly expands into the telencephalon of $Dmrta2^{-/-}; Pax6^{sey/sey}$ embryos. The PSB region is indicated by a dashed line. Arrows point to the limit of the expansion of *Gsx2* expression within the dorsal telencephalon. Scale bar, 500 μ m. An analysis of *Gsx1* expression in embryos of the same genotype is presented in Extended Data Figure 1-2. **C**, Coronal sections through the brain of E11.5 embryos of the indicated genotype processed by ISH for the expression of *Wnt3a* marking the hem. Arrowheads indicate the dorsal extent of *Wnt3a* expression in the medial pallium detected in $Dmrta2^{-/-}; Pax6^{sey/+}$ and $Dmrta2^{-/-}; Pax6^{sey/sey}$. h, hem. Scale bar, 500 μ m. Quantitative RT-qPCR analysis of *Wnt3a* in dissected cortices of $Dmrta2^{-/-}$, $Dmrta2^{-/-}; Pax6^{sey/+}$, and WT control embryos is shown on the left. Results are normalized to the level of the expression detected in the cortex of WT embryos. *** $p < 0.001$, Student's *t* test. Note that the reduction of *Pax6* partially rescues cortical hem formation in *Dmrta2* homo- and heterozygous mutant embryos. A similar analysis of *Wnt8b* expression in $Dmrta2^{+/-}$ embryos and in $Dmrta2^{+/-}$ embryos with one or two *Pax6^{sey}* alleles is presented in Extended Data Figure 1-3.

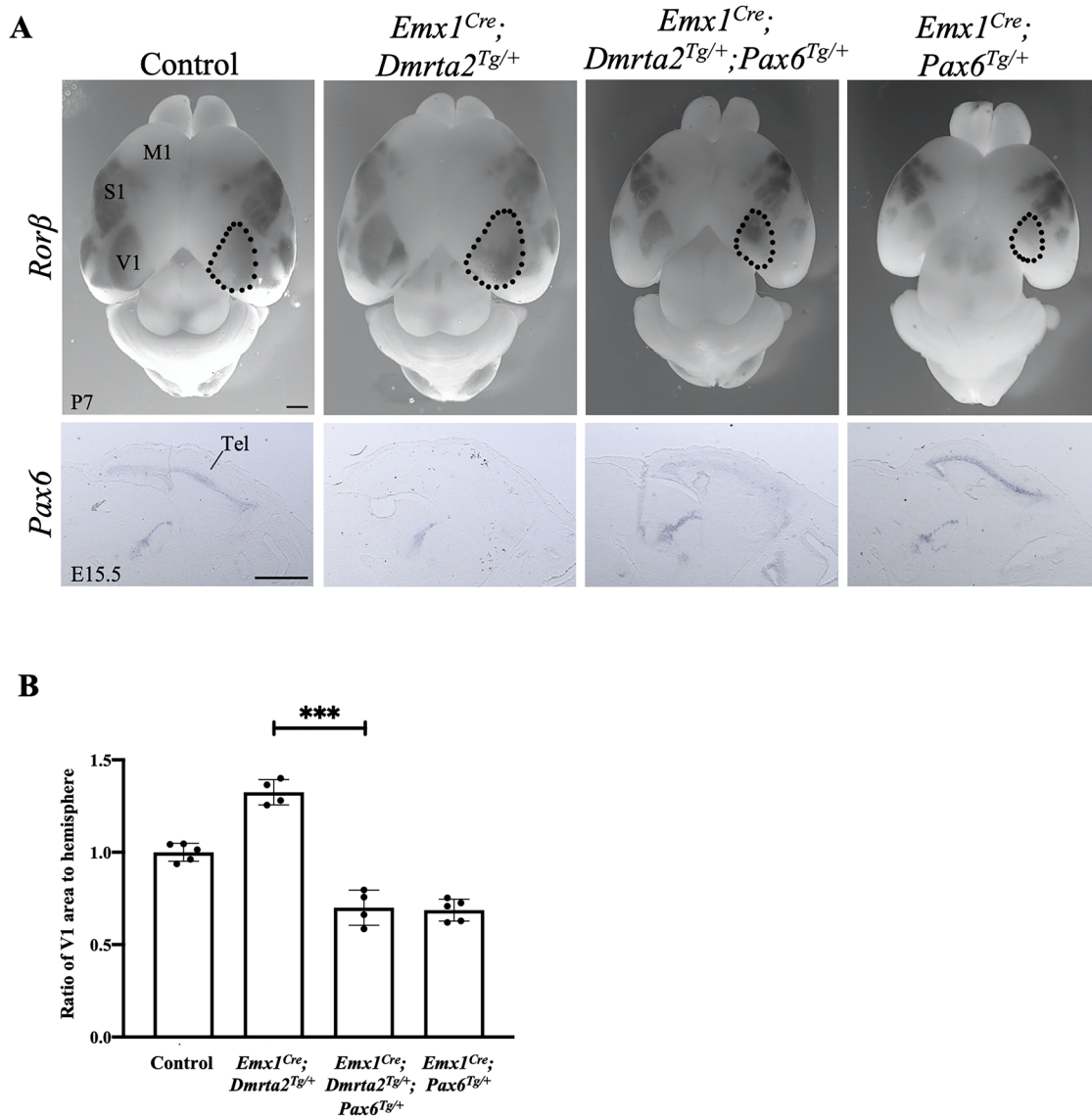
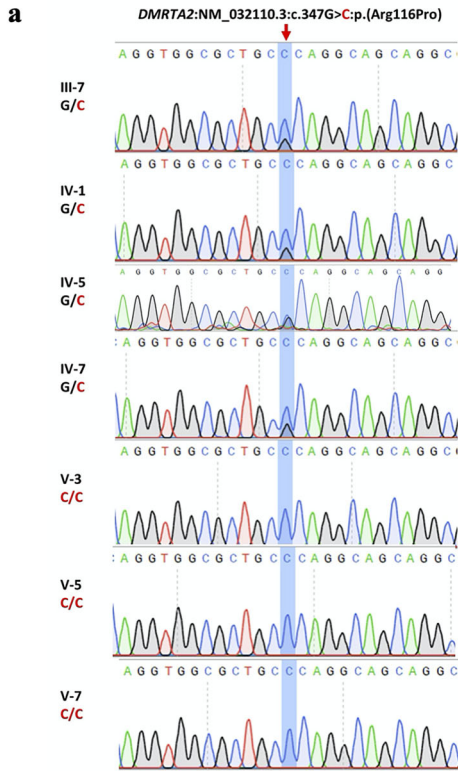


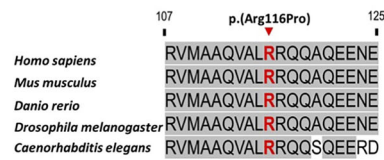
Figure 2. *Pax6* overexpression rescues the expansion of the V1 area observed in *Dmrta2* overexpressing transgenics. **A**, Dorsal views of the brain of P7 neonates of the indicated genotype processed by whole-mount ISH for *Rorb* expression. *Dmrta2^{Tg/+};* *Pax6^{Tg/+}* were used as controls. Sagittal sections of the brain of E15.5 embryos of the corresponding genotype with *Pax6* expression detected by ISH are shown below. Tel, telencephalon; M1, primary motor area; S1, primary somatosensory area; V1, primary visual areas. Scale bar, 100 μ m. **B**, Histograms show that as a ratio of surface area to total hemisphere size, V1 expansion is significantly rescued by the reduction of *Pax6*. *** $p < 0.001$, Student's *t* test.

be detected from E10.5 in Wnt reporter *BAT-gal* mice (Maretto et al., 2003; Extended Data Fig. 3-1), suggesting *Pax6* is a direct *Dmrta2* target. In accordance, ChIP-seq experiments have revealed that *Dmrta2* binds to the *Pax6* E60 enhancer, an ultraconserved cis-regulatory region located 25 kb downstream of *Pax6* in the large final intron of the adjacent *Elp4* gene, that contains several potential *Dmrta2* binding sites and drives complex expression of *Pax6* within the nervous system, including in the telencephalon (McBride et al., 2011; Konno et al., 2019). To address the possibility that *Dmrta2* affects *Pax6* E60 enhancer activity and investigate its mechanism of action, we performed transfection experiments in P19 mouse pluripotent embryonal carcinoma cells that have neurogenic potential (Farah et al., 2000). We have selected this cell line as it expresses at high levels early neural marker such as Sox2 but not *Pax6* (Babuska et al., 2010; Leszczyński et al., 2020) nor, most likely, *Dmrta2* and has been used previously for in vitro studies on enhancer activation by cortical transcription factors (Mariani et al., 2012; Pattabiraman et al., 2014). We transfected P19 cells with a luciferase reporter construct driven by a minimal tk promoter linked to the *Pax6* E60 enhancer. As *Pax6* autoregulates its expression (Aota et al., 2003), we transfected either naive or *Pax6* overexpressing cells with this reporter, in the absence or presence of *Dmrta2* expression vectors. We found that while *Pax6* overexpression had no significant effect on the control enhancer-less tk-luc reporter, it increased the activity of the E60 enhancer. In the presence of *Pax6*, we found that *Dmrta2* represses the activity of the E60 enhancer in a dose-dependent manner (Fig. 3A). Such repression was not observed with cotransfection of a construct

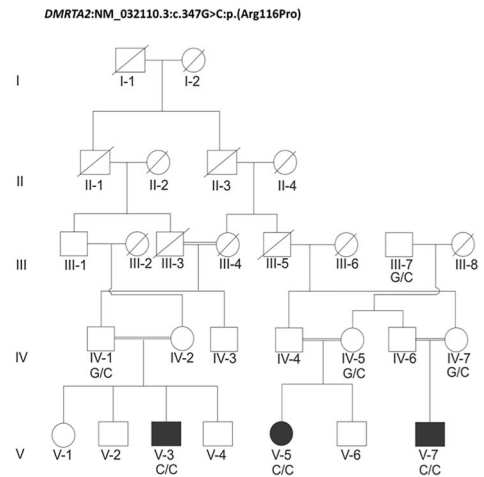
A



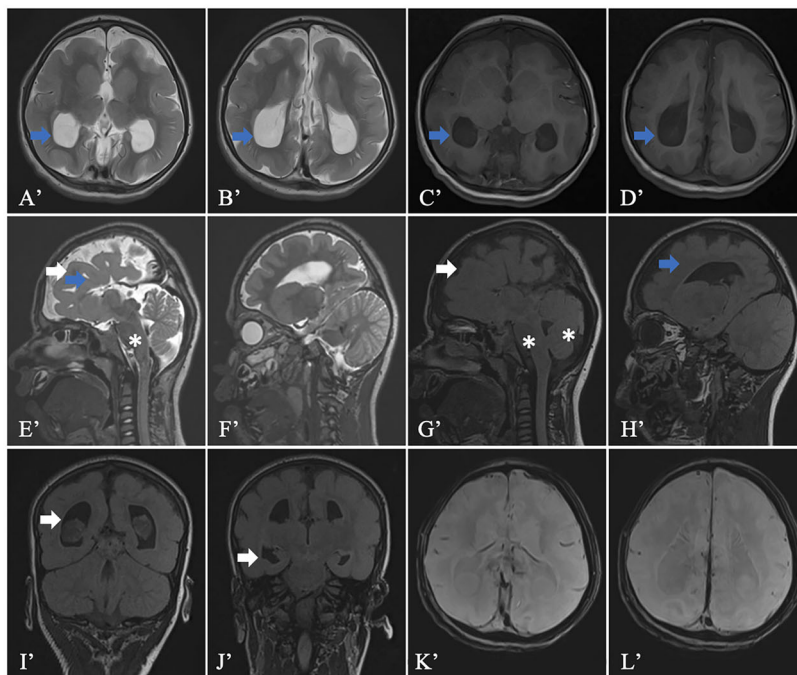
b



c



B



C

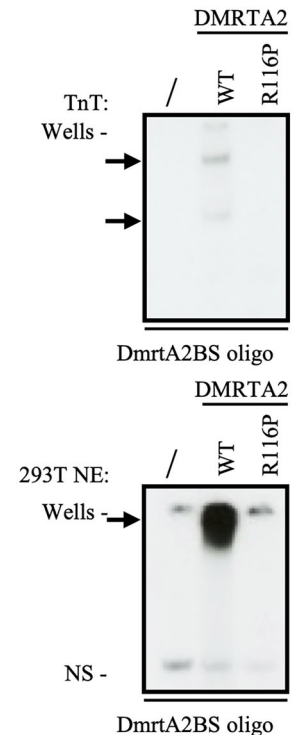


Figure 4. The homozygous missense variant in *DMRTA2* causes microcephaly in human. **A**, Sanger sequencing chromatograms (**a**) showing de novo G to C heterozygous and homozygous changes in sequence causing p.Arg116Pro coding change in *DMRTA2* identified in individuals of a consanguineous family. An alignment of the sequence of the central portion of the major groove recognition helix of human, murine fish, *Drosophila*, and *C. elegans* *Dmrt2* is shown (**b**), together with the pedigree (**c**) of the Pakistan family in which the mutation has been identified. Symbols marked by a slash indicate that the subject is deceased. Males are indicated by squares; females are indicated by circles. Blackened symbols represented individuals who were

performed in V-5, which revealed abnormalities indicating a mild encephalopathy. Full details of the clinical and genetic characterization of the V-3 and V-5 patients are provided in Extended Data Table 4-1.

Whether this mutation affects the activity of the protein is an important question to address. Therefore, we first asked whether the mutation affects the subcellular localization of the protein. When overexpressed as a flag fusion in human embryonic kidney HEK293T cells, we found that the mutated protein remains mainly nuclear (data not shown). Since *Dmrta2* functions as a DNA-binding transcription repressor, we then tested the ability of the mutated version to bind DNA by EMSA. To do so, we incubated the radiolabeled *Dmrta2* binding site (*Dmrta2*BS) probe (Murphy et al., 2007), known to bind the *Dmrta2*, with either nuclear extracts from HEK293T cells transfected with the expression vector of either the *DMRTA2*^{R116P} or the WT proteins or with either the *DMRTA2*^{R116P} or the WT proteins produced in vitro in rabbit reticulocyte lysates. We found that the *DMRTA2*^{R116P} mutated protein is unable to bind DNA (Fig. 4C). With this in vitro evidence of the plausible pathogenicity of the *DMRTA2*, *p.(Arg116Pro)* *VUS*, this variant can thus be reclassified as likely pathogenic following the updated ACMG criteria (PS3, PM2, PP1, PP3, and PP4). Together, these results suggest that *DMRTA2*^{R116P} causes cortical malformations by affecting its DNA binding properties.

Dmrta2 interacts with the NurD complex and Zfp423

How *Dmrta2* represses gene expression is unknown. To identify *Dmrta2* interacting partners, we generated transgenic mice expressing *Dmrta2* with an N-terminal 2× HA epitope using the CRISPR/Cas9 gene editing system (*Dmrta2*^{2XHA}). Figure 5A shows RT-qPCR, Western blot, and immunostaining experiments demonstrating that the tagged *Dmrta2* allele is expressed in the telencephalon of *Dmrta2*^{2XHA} embryos. We then performed rapid immunoprecipitation followed by mass spectrometry analysis of endogenous protein (RIME) experiments using anti-HA antibodies on chromatin extracts prepared from dissected dorsal cortices from E12.5 *Dmrta2*^{2XHA} and WT control embryos. As this method uses formaldehyde fixation to stabilize protein complexes, it is particularly suited to study chromatin and transcription factor complexes (Mohammed et al., 2016). Among the 263 proteins that selectively copurified with *Dmrta2*-HA (Fig. 5B), the major protein present in the *Dmrta2*^{2XHA} sample was *Dmrta2* in two independent replicates. Other members of the *DmrtA* family, such as *Dmrt3* and *Dmrt1*, were also efficiently recovered, which is expected given the ability of *DmrtA* proteins to bind DNA, forming homo- and heterodimers, trimers, or tetramers (Murphy et al., 2007, 2015). Interestingly, several components of the nucleosome remodeling and deacetylase NuRD complex (including CHD4, HDAC1/2, MBD3, among others; Nitarska et al., 2016) and the vertebrate-specific zinc finger transcription factor *Zfp423/ZNF423* (also termed OLF/EBF associated-zinc finger protein OAZ) and its homolog *Zfp521* that interact with the NuRD complex (Harder et al., 2014; Li et al., 2021; Shao et al., 2021) and regulate neurogenesis (Cheng et al., 2007; Kamiya et al., 2011; Shen et al., 2011; Ohkubo et al., 2014; Shahbazi et al., 2016; Massimino et al., 2018) were also selectively enriched in the *Dmrta2*^{2XHA} samples (Fig. 5C,D; Extended Data Fig. 5-1). Among the other proteins recovered selectively in the *Dmrta2*^{2XHA} sample was the zinc-finger protein *Zfp462* which regulates neural lineage specification by targeting the H3K9-specific histone methyltransferase complex G9A/GLP to silence meso-endodermal genes (Yelagandula et al., 2023) and the E3 ubiquitin ligases BRE1a and BRE1b that regulate the cell cycle and differentiation of neural precursor cells (NPCs) through monoubiquitylation of histone H2B (Ishino et al., 2014).

Zfp521 can act as a repressor or activator depending on the cellular context (Scicchitano et al., 2019; Chiarella et al., 2021). During the differentiation of embryonic stem cells into neural progenitors, *Zfp521* has been shown to act mainly as an activator of neural genes (Kamiya et al., 2011). *Zfp462* has been shown to repress mesoendodermal genes during neural differentiation of embryonic stem cells but does not affect *Pax6* upregulation (Yelagandula et al., 2023). Therefore, and based on our data showing that *Dmrta2* complexes contain multiple NuRD subunits, we focused on the NuRD-interacting *Zfp423* protein as a possible *Dmrta2* interacting partner potentially involved in its repressive function. By in situ hybridization and immunostaining, we found as previously reported (Cheng et al., 2007; Massimino et al., 2018) that *Zfp423* is expressed in cortical progenitors, the highest expression being detected in the hem region (Fig. 5E). To further investigate the ability of *Dmrta2* to form a complex with *Zfp423*, constructs encoding *Zfp423* and Flag-tagged *Dmrta2* were cotransfected in HEK293T cells. In Co-IP assays, results obtained indicated that Flag-*Dmrta2* interacts with *Zfp423* (Fig. 6A) and that a *Dmrta2* DM domain deletion mutant (Flag-*Dmrta2*ΔDM) does not bind to *Zfp423*, revealing that the DM domain of *Dmrta2* is required for the interaction (Fig. 6B). GST pull-down experiments were also performed using three purified GST-fusion proteins: one encoding the full-length m*Dmrta2*, another the m*Dmrta2* DM alone, and a third one encoding the related m*Dmrt3* protein. Mouse *Zfp423* has been produced by in vitro

←
identified as patients according to clinical examination. **B**, Magnetic resonance (MRI) images of the brain phenotype. First row, Axial T2-weighted (**A**, **B**) and T1-weighted (**C**, **D**) images showing, colpocephaly, i.e., dilated posterior horns (blue arrows), with relatively parallel orientation of the bilateral lateral ventricles suggestive of complete agenesis of the corpus callosum. Second row, Sagittal T2-weighted (**E**, **F**) and T1-weighted (**G**, **H**) images showing pachygyria (white arrows) and absent cingulate gyrus (blue arrows). The brainstem and cerebellum are normal (white asterisks). Third row, Coronal fluid-attenuated inversion recovery (FLAIR) sequences (**I**, **J**), showing enlarged occipital as well as temporal horns with no periventricular white matter changes. Axial SWI (susceptibility weighted images; **K**, **L**) does not show any calcifications. Details of the clinical characterization of the V-3 and V-5 patients are provided in Extended Data Table 4-1. **C**, EMSA with a labeled DNA probe containing a *DMRTA2* consensus binding motif (*DmrtA2*BS) incubated with (top panel) *DMRTA2* WT or *DMRTA2*^{R116P} proteins produced by TnT and (bottom panel) nuclear extracts from HEK293T cells either nontransfected (**I**) or transfected with *DMRTA2* WT or *DMRTA2*^{R116P}. Proteins present in the binding reactions are indicated above. Arrows indicate the position of the DNA-protein complexes. "NS" indicates nonspecific complexes.

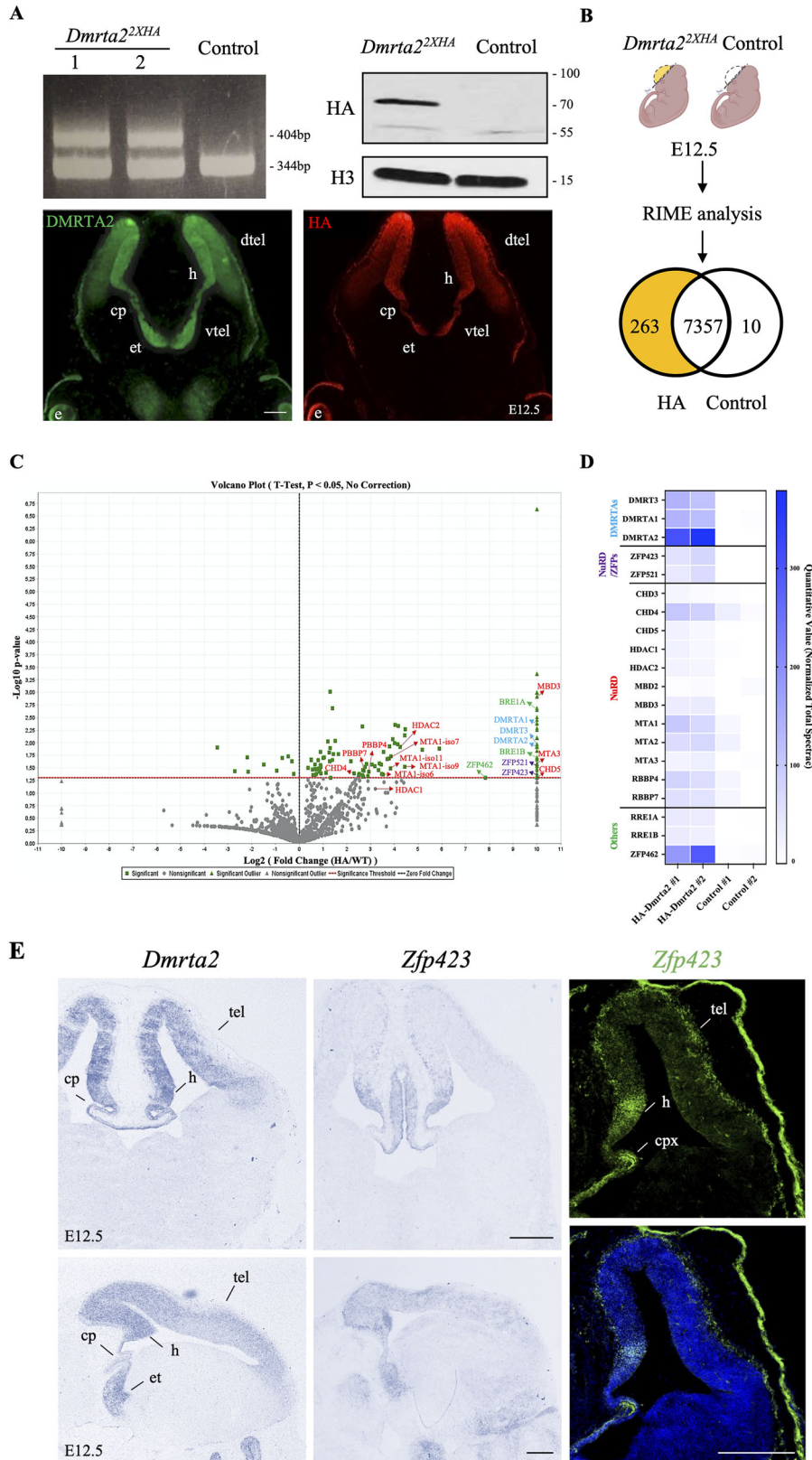


Figure 5. RIME-purified Dmrta2 complexes isolated from dissected cortical tissue contain multiple subunits of NuRD and the NuRD interacting Zfp423 protein. **A**, Top panels, RT-qPCR using cDNA prepared from dissected cortices of E12.5 embryos with primers flanking the inserted 2x HA sequence, showing that the tagged allele is detectable in the two F0 *Dmrta2*^{2XHA} mice (clones 1 and 2) and is absent in WT mice. A Western blot is also shown demonstrating that the HA-tagged protein is expressed in *Dmrta2*^{2XHA} mice. Bottom panels, immunostainings showing that the HA-tagged allele is expressed similarly to Dmrta2 in the telencephalon. h, hem; cp, choroid plexus; dtel, dorsal telencephalon; e, eye; et, eminentia thalami; vtel, ventral telencephalon.

transcription/translation and detected by western blot using anti-Zfp423 antibodies. As shown in Figure 6C, Zfp423 does not interact with purified GST alone but was recovered with the GST-Dmrta2, GST-Dmrta2 DM, and GST-Dmrt3 fusion proteins. These results confirm the ability of Dmrt transcription factors to interact with Zfp423 and show that the DM domain of Dmrta2 is sufficient for this interaction.

As Zfp423 interacts with the NuRD complex, its interaction with Dmrta2 may contribute to its repressive properties. To test this hypothesis, *Zfp423* was cotransfected at increasing doses with a fixed dose of Flag-*Dmrta2* in HEK293T cells. Co-IP assays were then performed using an anti-Flag antibody followed by Western blotting using antibodies for Flag-Dmrta2, Zfp423, and NuRD complex components. Despite some background binding observed with protein G magnetic beads alone used as a negative control, the results obtained show that Dmrta2 immunoprecipitate some NuRD subunits (i.e., HDAC1 and MBD3, compare levels in lines 1 and 5). With increasing doses of Zfp423, as expected, increasing binding of Zfp423 was observed. Interestingly, increased binding of Zfp423 to Dmrta2 appears to increase the amount of coimmunoprecipitated HDAC1/2 and MBD3 (Fig. 6D, Extended Data Fig. 6-1). To test the hypothesis that Dmrta2 represses its targets via the recruitment of NuRD components, we performed reporter assays with a *Pax6 E60-luc* reporter construct in P19 cells transfected as above with a *Pax6* expression vector to stimulate *E60* enhancer activity, in the presence or absence of cotransfected *Dmrta2*. Twenty-four hours after transfection, cells were treated with the class I HDAC inhibitor romidepsin, which is known for its selective inhibition of HDAC 1, 2, 3, and 8 (Petrich and Nabhan, 2016; Mayr et al., 2021). Results obtained showed that romidepsin significantly decreases the repressive effect of Dmrta2 and that such an effect is not observed in the absence of Dmrta2 (Fig. 6E). These data suggest that Dmrta2 functions as a transcriptional repressor through the recruitment of the NuRD complex.

To determine whether Zfp423 plays a role in Dmrta2 repressive function, we first examine the consequences of its overexpression on the ability of Dmrta2 to repress the E60 enhancer in P19 cells. Cotransfection of *Dmrta2* with an increasing amount of a *Zfp423* expression plasmid did not further decrease luciferase activity (Extended Data Fig. 6-2). As this may be due to the fact that Zfp423 is already strongly expressed in P19 cells (Masserdotti et al., 2010; Cho et al., 2013), to address a potential role for Zfp423 in Dmrta2 repressive function, we turned to HEK293T cells in which *Zfp423* is expressed at low level (proteinatlas.org). As the *Pax6 E60* enhancer is not active in HEK293T cells, we performed reporter assays with a luciferase reporter plasmid containing five GAL4 binding sites located upstream of a HSV tk promoter (5XUAS-tk-luc) and an expression construct encoding a chimeric protein consisting of the Gal4 DNA-binding domain fused to Dmrta2, in the presence or absence of MycZfp423. The results obtained (Fig. 6F) show that cotransfection of the expression construct encoding Gal4-Dmrta2 decreases luciferase activity, with a low amount of transfected Gal4-Dmrta2 expression vector sufficient to produce a ~10-fold decrease of luciferase activity. Such a strong decrease was not observed using a luciferase reporter plasmid without GAL4 binding sites upstream of a HSV tk promoter (Extended Data Fig. 6-3). Cotransfection of this Gal4-dependent luciferase reporter with an expression vector encoding Zfp423 at a high dose produced only a weak decrease (~2-fold). Notably, cotransfection of this *Zfp423* expression vector together with Gal4-Dmrta2 led to a slightly more pronounced decrease than that observed with Gal4-Dmrta2 alone (Fig. 6F). Such a cooperative repressive effect on 5XUAS-tk-luc was not observed when Myc-Zfp423 was cotransfected with a Gal4 DNA-binding domain alone expression vector, which we found to slightly decrease luciferase activity (Extended Data Fig. 6-4). As an additional control, to validate the modest cooperative effect observed when Zfp423 is coexpressed with Dmrta2, we also cotransfected Zfp423 with an expression vector encoding a Gal4-Dmrta2 mutant in which the N-terminal part containing the DM domain required for Zfp423 interaction has been deleted, Gal4-Dmrta2 (126–531). Results obtained show that, as observed with Dmrta2 wild type, Gal4DBD-Dmrta2 (126–531) also leads to a strong decrease of 5XUAS-tk luc activity. However, in contrast to the Dmrta2 full-length protein, cotransfection of Zfp423 with this Dmrta2 deletion mutant did not further decrease luciferase activity (Fig. 6F). Together, these results confirm the ability of Dmrta2 to mediate transcriptional repression. They reveal that regions downstream of the DM domain of Dmrta2 participate in its repressive properties and suggest that Zfp423 interacting with the DM domain contribute to Dmrta2 repression activity.

Discussion

In this study, we have investigated how Dmrta2 and Pax6, two transcription factors expressed in the cortical ventricular zone in opposite gradients, interact to control the spatiotemporal identity of neural progenitors and regulate regional

←

Scale bar, 200 μ m. **B**, Schematic diagram of the experiment performed. Cortices were dissected from E12.5 *Dmrta2*^{2xHA} and control embryos and subjected to RIME analysis. Venn diagrams with the number of the differentially copurified proteins identified in the cortex of *Dmrta2*^{2xHA} and control embryos are shown. **C**, A Volcano plot showing the identified Dmrta2 interacting proteins identified using RIME. All statistically validated proteins are represented by green points, while gray points represent background binding proteins. An arbitrary log₂ fold change value of 10 was attributed to the proteins detected only in the HA-Dmrta2 experimental conditions. Proteins of interest are indicated with name ($n = 3$ for each condition). Dmrta2 and other DMRTA family members are highlighted in bright blue, NuRD members in red, and NuRD complex interacting zinc-finger proteins in orange. **D**, A heatmap showing the significantly enriched proteins identified by RIME and their normalized total spectral count across indicated samples ($n = 2$ for each condition). Peptide coverage for some of the identified Dmrta2 interacting proteins is presented in Extended Data Figure 7-1. **E**, ISH on coronal (left top panels) and sagittal (left bottom panels) sections of the brain of a E12.5 embryo for *Dmrta2* and *Zfp423* and IF with Zfp423 antibodies on a coronal section through the dorsal telencephalon of a E12.5, without or with DAPI counterstaining (right panels) showing that *Zfp423* is coexpressed with *Dmrta2* in the mouse embryonic cortex. Cp, choroid plexus; et, eminentia thalami; h, hem; tel, telencephalon; Scale bar, 200 μ m.

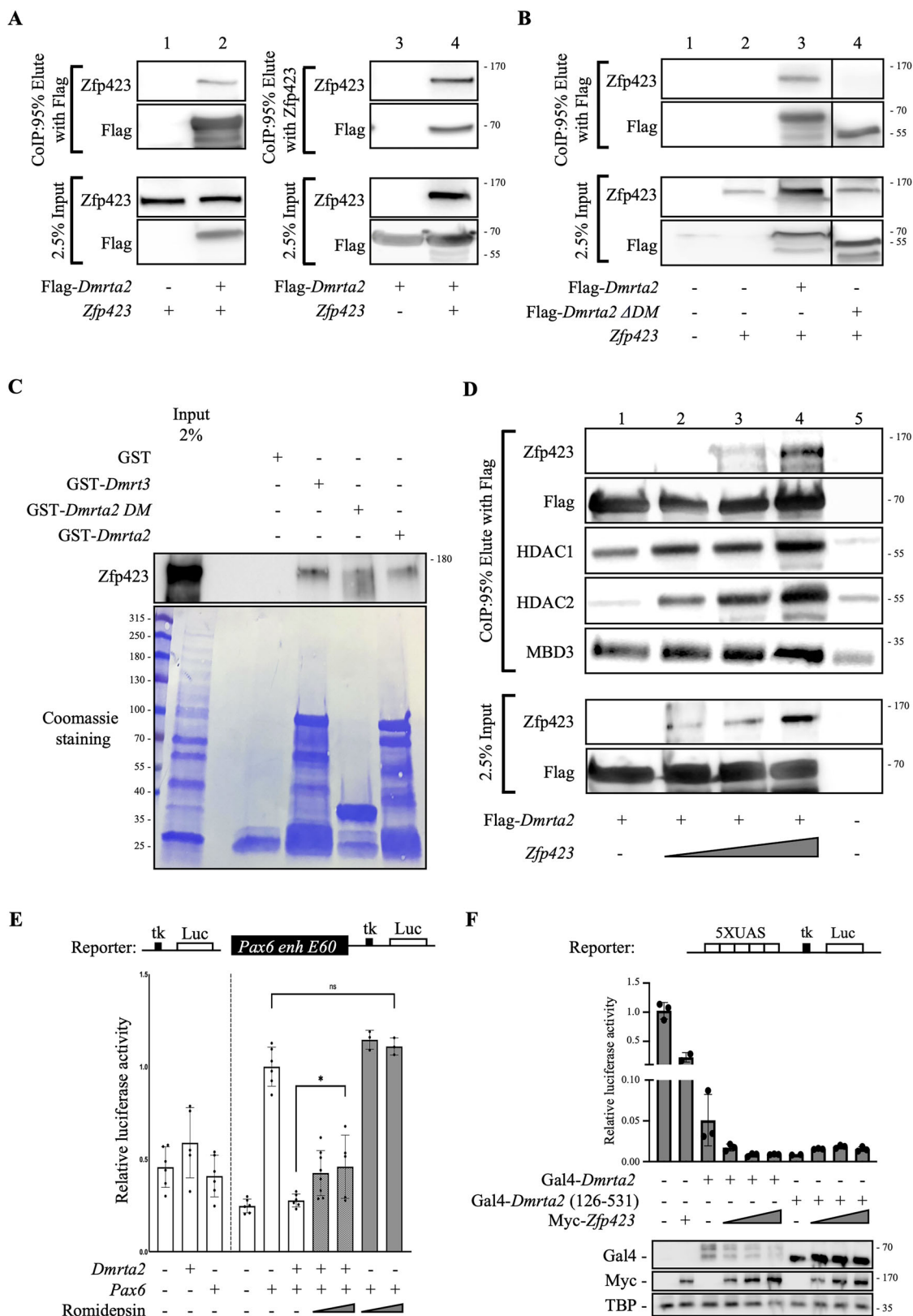


Figure 6. The Dmrta2-Pax6 interaction requires the recruitment of the HDAC-NuRD complex by Zfp423. **A, B**, Coimmunoprecipitation assays as indicated with Zfp423, Flag-Dmrta2, and a Flag-Dmrta2 mutant lacking the DM domain (Flag-Dmrta2 ΔDM) overexpressed in HEK293T cells as indicated. Note in **A** that Flag-Dmrta2 pulled down Zfp423 (line 1–2) and that, conversely, Zfp423 coprecipitated Flag-Dmrta2 (line 3–4). Note in **B** that Flag-Dmrta2 ΔDM does not pull down Zfp423 (line 4). *n* = 3. Segments from the same blot have been spliced together to show side by side the results of the WT and the ΔDM Dmrta2 mutant. **C**, Full-length mouse Myc-tagged Zfp423 was synthesized in vitro and incubated with GST alone or with GST fusion proteins bound to

neurogenesis. We show that *Pax6* is already upregulated by the loss of *Dmrt2* at E9.5 before the disruption of Wnt signaling, in accordance with its identification as a *Dmrt2* direct target (Konno et al., 2019). *Pax6* promotes neurogenesis while *Dmrt2* maintains neural progenitors in the cell cycle (Scardigli et al., 2003; Sansom et al., 2009; Young et al., 2017). We found that the absence of one allele of *Pax6* partially rescues the reduction of the size of the cortex observed in *Dmrt2*^{-/-} embryos due to premature neuronal differentiation. This is in accordance with the observation that the siRNA knockdown of *Pax6* expression in medial cortical cells electroporated with siRNAs targeting *Dmrt3* and *Dmrt2* rescues their neurogenic phenotype.

Both *Pax6* (Toresson et al., 2000; Yun et al., 2001; Carney et al., 2009; Sun et al., 2015) and *Dmrt2* (Desmaris et al., 2018; Konno et al., 2019) have been reported to be required for defining the dorsal telencephalic compartment and directly repress *Gsx1* and *Gsx2*. *Pax6* function in dorsoventral telencephalon patterning may also occur through another member of the *Dmrt* family, *Dmrt1*, as it is positively regulated by *Pax6* and that its overexpression in the ventral telencephalon induces the expression of the dorsal proneural factor *Neurog2* and represses the ventral marker *Ascl1* (Kikkawa et al., 2013). Here we show that the subpallial markers *Gsx2* but also *Gsx1* are robustly ectopically expressed in the abortive cortical primordium of *Pax6*; *Dmrt2* double KO embryos, a phenotype not observed in single KO, indicating that *Dmrt2* and *Pax6* cooperation is essential for maintaining cortical identity in dorsal telencephalic progenitors. Such a phenotype is not observed in *Dmrt2*^{-/-}; *Pax6*^{sey/+} mutants suggesting that a low amount of *Pax6* is sufficient to repress *Gsx1* and *Gsx2* expression. Thus, *Gsx1* and *Gsx2* appear to be particularly sensitive to *Pax6*, as *Gsx2* is to *Dmrt* factors (Konno et al., 2019). The combined loss of *Pax6* and *Emx2* (Muzio et al., 2002b) and of *Dmrt2* and *Emx2* (Desmaris et al., 2018) also results in the ectopic expression of ventral-specific markers in the dorsal telencephalon. Early telencephalon dorsoventral patterning and the maintenance of the identity of cerebral cortical progenitors appear thus to be under the tight control of multiple cortical factors that cooperate to repress the expression of a set of ventral telencephalic determinants, including *Gsx1* and *Gsx2*.

Pax6 is expressed in a rostromedial^{high}/caudomedial^{low} gradient, opposite to that of *Dmrt2*. *Pax6* regulates dorsoventral patterning in the telencephalon. Within the lateral telencephalon, *Pax6* contributes to the restriction of medial cortical fate (Muzio et al., 2002a; Godbole et al., 2017). *Pax6* also promotes a rostral fate in cortical progenitors. In small eye mutants that lack functional *Pax6* protein, caudal visual areas are expanded (Bishop et al., 2000; 2002). The cortex-specific deletion or overexpression of *Pax6* has been also shown to reduce S1 area size (Manuel et al., 2007; Zembrzycki et al., 2013). The study by Konno et al. (2019) suggested that the graded expression of *Dmrt* factors repressing *Pax6* transcription and thus establishing its lateral^{high}/medial^{low} expression gradient provides mediolateral positional information to cortical progenitors. Our findings that the loss of one allele of *Pax6* partially rescues medial cortical hem in *Dmrt2* hetero- and homozygous mutant embryos provide first in vivo experimental evidence supporting this model. It suggests that a higher amount of *Pax6* is needed within the cortical primordium to repress hem fate than to repress *Gsx2*, suggesting that some *Pax6* targets are also differentially sensitive to its dosage. In the developing mouse lens, *Six3* expression has been shown to be dose dependent on *Pax6* function (Goudreau et al., 2002). Our observation that *Pax6* overexpression rescues the expansion of V1 area observed in *Dmrt2* overexpressing transgenics further demonstrates the importance of the repressive action of *Dmrt* factors on *Pax6* in positional information of cortical progenitors. Together, our data are in agreement with the model proposed by Konno et al. (2019) suggesting *Dmrt5* acts mainly by differential suppression of *Pax6* and other homeobox transcription factors. A summary of the interactions identified in this work and in previous studies between *Dmrt2* and related family members and *Pax6* in cortical patterning is shown in Figure 7. Sexual differences are prevalent in the brain. *DMRT* transcription factors have been postulated as important determinants of sex differences (Casado-Navarro and Serrano-Saiz, 2022). A recent study has shown that one alternative transcript

←
glutathione-agarose beads as indicated. Bound Myc-tagged Zfp423 was detected by immunoblot with an anti-Myc antibody. A 2% input sample was loaded for comparison. The corresponding Coomassie-stained gel is shown. *n* = 2. **D**, Coimmunoprecipitation assays as indicated with HEK293T cells transfected with a Flag-*Dmrt2* expression construct, alone or together with increasing doses of a *Zfp423* expression construct. Note that *Dmrt2* immunoprecipitates some NuRD subunits and that the binding of *Zfp423* to *Dmrt2* increases the amount of coimmunoprecipitated HDAC1/2 and MBD3. Densitometric quantification of the western blot results is shown in Extended Data Figure 6-1. *n* = 3. **E**, Reporter assays in P19 cells transfected with a *Pax6* E60 tk-luc reporter vector, or an “empty” tk-luc reporter vector as indicated, together with a pCS2Myc-*Pax6* expression vector and/or a pCS2Flag-*Dmrt2* expression vector as indicated, in the absence (white bars) or presence of increasing doses of the HDAC1 inhibitor romidepsin (gray bars). Note that romidepsin leads to a stronger increase of luciferase activity reaching significance in the presence of *Dmrt2* but not in its absence. The mean activity of the *Pax6* E60 enhancer reporter construct with cotransfected *Pax6* is set to 1. NS, not significant. **p* < 0.05, one-way ANOVA test. Results of similar reporter assays performed in P19 cells, in the presence or absence of *Zfp423* are presented in Extended Data Figure 6-2. **F**, Reporter assays in HEK293T cells show that both Gal4-*Dmrt2* and the Gal4-*Dmrt2* (126–531) fusion construct lacking the DM domain required for *Zfp423* interaction has strong repression activity on the 5XUAS-tk-luc reporter construct and that *Zfp423* slightly increases the repressive activity of Gal4-*Dmrt2* but not of the Gal4-*Dmrt2* (126–531) construct. In each condition, 200 ng of the 5XUAS-tk-luc reporter was transfected, together with 25 ng of the pCMV-Gal4-*Dmrt2* or the pCMV-Gal4-*Dmrt2* (126–531) and different doses (200, 400 and 600 ng) of pCDNA3-Myc-*Zfp423* expression plasmids. Values represent the mean ± SD of one transfection done in triplicate. A Western blot showing the expression levels of the overexpressed factors is shown below. Reporter assays showing that the Gal4-*Dmrt2* fusion protein represses in a UAS-dependent manner the activity of the 5XUAS-tk-luc reporter are presented in Extended Data Figure 6-3. Reporter assays in HEK293T cells showing that *Zfp423* does not increase the modest repression observed when an expression vector encoding the Gal4 DNA-binding domain alone is cotransfected with the 5XUAS-tk-luc reporter are presented in Extended Data Figure 6-4.

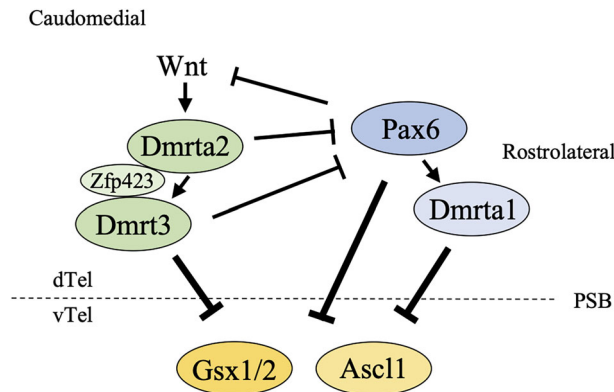


Figure 7. Model illustrating the action of Dmrta2 and related family members in cortical patterning. Our results provide experimental evidence showing that downstream of hem derived Wnt signals, Dmrta2 acts through the repression of Pax6 to promote caudomedial fate, and it cooperates with Pax6 to repress ventral determinants such as Gsx1 and Gsx2, extending previous studies having defined Pax6 regulation by Dmrt factors (Konno et al., 2012; Saulnier et al., 2013; Young et al., 2017). In accordance with Konno et al. (2019), the data suggest that Dmrta2 interacting with Zfp423 and the NuRD complex differentially repress the expression of Pax6 and Gsx1/2. Greater or lesser Dmrt repression capacity is indicated by thick or thin repression arrows, respectively. Similarly, Gsx1 and Gsx2 appear more sensitive to Pax6 than Wnt3a in the hem. Dmrta3 that is regulated by Dmrta2 contributes to the repression of Pax6 (De Clercq et al., 2016). Dmrta1 that is upregulated by Pax6 contributes to its ability to repress ventral telencephalic genes such as Asc11 (Kikkawa et al., 2013). PSB, pallium subpallium boundary; dTel, dorsal telencephalon; vTel, ventral telencephalon.

of another member of the DM family, Dmrta2, is slightly more expressed (1.67 times more) in the developing cingulate cortex at E13.5 in males than in females and that its downregulation results in a more pronounced decrease of cingulate cortex neural precursors in male embryos (Bermejo et al., 2025). Although *Dmrta2* has not been identified as a differentially expressed gene showing sex differential expression in recent studies by RNAseq of the developing mouse cortex (Ochi et al., 2024) or during neural differentiation of human embryonic stem cells (Pottmeier et al., 2024), it appears to be transiently expressed at a slightly higher level (1.2 \times) in males than in females at E11.5. Whether this subtle difference in *Dmrta2* expression between male and female can lead to significant distinct outcomes in cortex development between sexes remains to be explored.

How Dmrta2 represses its targets in cortical progenitors and how it does it in a dose-dependent manner remains today unknown. Therefore, we performed reporter gene assays in P19 cells using the Pax6 E60 enhancer. Given the low activity of this enhancer in P19 cells, those assays were done in the presence of Pax6, as previous studies reported that Pax6 autoregulates its expression (Aota et al., 2003; Manuel et al., 2007, 2015) and that Pax6 binds to this enhancer region (Sun et al., 2015). In accordance with these studies, our results show that Pax6 increases luciferase activity using this E60 enhancer-driven reporter construct. However, this is not in agreement with the observation that this E60 enhancer remains active in Pax6^{sey/sey} mutants (McBride et al., 2011). The reason for this discrepancy remains unclear. Our results indicate that Dmrta2 counteracts the activation by Pax6 of this E60 enhancer-driven reporter and that the zinc finger motifs of Dmrta2 that are required for DNA binding (Murphy et al., 2015) are essential for this repression. These results suggest that Dmrta2 acts as a DNA-binding repressor on the Pax6 locus, as it appears to be the case on the repressor of neurogenesis *Hes1* and on the Gsx2 genomic loci (Young et al., 2017; Desmaris et al., 2018). This is also further supported by the identification of the human DMRTA2^{R116P} point mutation reported here that, to our knowledge, is the only mutation in DMRTA2 suggested to play a role in microcephaly by affecting its ability to bind DNA. The DMRTA2^{R116P} mutation corresponds to DMRT1^{R/K122} involved in DNA phosphate backbone contacts. The fact that the change is to a proline, a helix-breaking residue, and occurs close to DMRT1^{R123} that makes base-specific contacts likely explains the observed disruption of DNA binding. An animal model of the DMRTA2^{R116} mutation may help to elucidate the cause of the phenotype observed in this family.

One critical step in the understanding of the mode of action of a transcription factor is the identification of the protein complexes in which it acts. Our data indicate that Dmrta2 interacts with the NuRD complex and with the multizinc finger Zfp423 and related Zfp521 proteins that are expressed in cortical progenitors (Kamiya et al., 2011; Massimino et al., 2018) and themselves interact with NuRD components (Harder et al., 2014; Li et al., 2021; Shao et al., 2021). They show that Dmrta2 associates with Zfp423 via its DM domain and suggest that the recruitment of Zfp423 modestly contributes to Dmrta2's repressive properties. We found however that regions downstream of the DM domain of Dmrta2 also acts as a repressor domain, indicating that Zfp423 although contributing to is not obligatory for Dmrta2 repressive properties.

Although further studies are needed to demonstrate that Zfp423 and related Zfp521 interact with Dmrta2 in cortical progenitors and help it to repress some of its targets, they appear as potential candidate Dmrt interacting partners. Indeed, Zfp423 and Zfp521 both play important roles in neural development. The importance of Zfp521 for neural development is demonstrated by the fact that it is essential and sufficient for driving the intrinsic neural differentiation of mouse ES cells

(Kamiya et al., 2011; Shahbazi et al., 2016). ZNF423 mutations are associated with Joubert Syndrome, a ciliopathy causing cerebellar vermis hypoplasia and ataxia. Null Zfp423 mutants develop cerebellar malformations and hindbrain choroid plexus hypoplasia (Cheng et al., 2007; Casoni et al., 2017, 2020). In the forebrain, the corpus callosum is absent and the hippocampus is reduced. The cortex is thinner than the controls due to reduced proliferation. When Zfp423 is over-expressed in the cortex of E13.5 mouse embryos, it increases the number of electroporated cells positive for the neuronal marker *Tubb3* at the expense of mitotically active PAX6⁺ radial glia cells (Alcaraz et al., 2006; Massimino et al., 2018). Whether these changes in cell proliferation and differentiation upon manipulation of Zfp423 expression are linked to its interaction with Dmrt2 or, alternatively, to its ability to modulate other signaling pathways, like the SMAD/BMP, NOTCH, and SHH pathways (Hata et al., 2000; Ku et al., 2006; Masserdotti et al., 2010; Hong and Hamilton, 2016), remains to be elucidated.

Data Availability

All data used in the preparation of this manuscript will be provided upon request.

References

- Alcaraz WA, Gold DA, Raponi E, Gent P, Conception D, Hamilton BA (2006) Zfp423 controls proliferation and differentiation of neural precursors in cerebellar vermis formation. *Proc Natl Acad Sci U S A* 103:19424–19429.
- Aota SI, Nakajima N, Sakamoto R, Watanabe S, Ibaraki N, Okazaki K (2003) Pax6 autoregulation mediated by direct interaction of Pax6 protein with the head surface ectoderm-specific enhancer of the mouse Pax6 gene. *Dev Biol* 257:1–13.
- Babuska V, Kulda V, Houdek Z, Pesta M, Cendelin J, Zech N, Pachernik J, Vozeh F, Uher P, Kralickova M (2010) Characterization of P19 cells during retinoic acid induced differentiation. *Prague Med Rep* 111:289–299.
- Berger J, Berger S, Tuoc TC, D'Amelio M, Cecconi F, Gorski JA, Jones KR, Gruss P, Stoykova A (2007) Conditional activation of Pax6 in the developing cortex of transgenic mice causes progenitor apoptosis. *Development* 134:1311–1322.
- Bermejo A, Torrilas-de la Cal R, Rubio-Garcia M, Serrano-Saiz E (2025) Dmrt2 orchestrates neuronal development in the embryonic cingulate cortex: unavailing sex biased vulnerabilities. *BioRxiv*.
- Bishop KM, Goudreau G, O'Leary DD (2000) Regulation of area identity in the mammalian neocortex by Emx2 and Pax6. *Science* 288:344–349.
- Bishop KM, Rubenstein JL, O'Leary DD (2002) Distinct actions of Emx1, Emx2, and Pax6 in regulating the specification of areas in the developing neocortex. *J Neurosci* 22:7627–7638.
- Cadwell CR, Bhaduri A, Mostajo-Radji MA, Keefe MG, Nowakowski TJ (2019) Development and arealization of the cerebral cortex. *Neuron* 103:980–1004.
- Carney RS, Cocas LA, Hirata T, Mansfield K, Corbin JG (2009) Differential regulation of telencephalic pallial–subpallial boundary patterning by Pax6 and Gsh2. *Cereb Cortex* 19:745–759.
- Casado-Navarro R, Serrano-Saiz E (2022) DMRT transcription factors in the control of nervous system sexual differentiation. *Front Neuroanat* 16:937596.
- Casoni F, Croci L, Bosone C, Hawkes R, Warning S, Consalez GG (2017) Zfp423/ZNF423 regulates cell cycle progression, the mode of cell division and the DNA-damage response in Purkinje neuron progenitors. *Development* 144:3686–3697.
- Casoni F, Croci L, Vincenti F, Podini P, Riba M, Massimino L, Cremona O, Consalez GG (2020) ZFP423 regulates early patterning and multiciliogenesis in the hindbrain choroid plexus. *Development* 147:dev190173.
- Cheng LE, Zhang J, Reed RR (2007) The transcription factor Zfp423/OAZ is required for cerebellar development and CNS midline patterning. *Dev Biol* 307:43–52.
- Chiarella E, Aloisio A, Scicchitano S, Todoerti K, Cosentino EG, Lico D, Neri A, Amodio N, Bond HM, Mesuraca M (2021) ZNF521 enhances MLL-AF9-dependent hematopoietic stem cell transformation in acute myeloid leukemias by altering the gene expression landscape. *Int J Mol Sci* 22:10814.
- Cho YW, Hong CJ, Hou A, Gent PM, Zhang K, Won KJ, Hamilton BA (2013) Zfp423 binds autoregulatory sites in p19 cell culture model. *PLoS One* 8:e66514.
- De Clercq S, et al. (2018) DMRT5 together with DMRT3 directly controls hippocampus development and neocortical area map formation. *Cereb Cortex* 28:493–509.
- Desmaris E, et al. (2018) DMRT5, DMRT3, and EMX2 cooperatively repress GSX2 at the pallium–subpallium boundary to maintain cortical identity in dorsal telencephalic progenitors. *J Neurosci* 38:9105–9121.
- Dignam JD, Lebovitz RM, Roeder RG (1983) Accurate transcription initiation by RNA polymerase II in a soluble extract from isolated mammalian nuclei. *Nucleic Acids Res* 11:1475–1489.
- Farah M, Olson JM, Susic HB, Hume RI, Tapscott SJ, Turner DL (2000) Generation of neurons by transient expression of neural bHLH proteins in mammalian cells. *Development* 127:693–702.
- Godbole G, Roy A, Shetty AS, Tole S (2017) Novel functions of LHX2 and PAX6 in the developing telencephalon revealed upon combined loss of both genes. *Neural Dev* 12:1–8.
- Goudreau G, Petrou P, Reneker LW, Graw J, Löster J, Gruss P (2002) Mutually regulated expression of Pax6 and Six3 and its implications for the Pax6 haploinsufficient lens phenotype. *Proc Natl Acad Sci U S A* 99:8719–8724.
- Hamasaki T, Leingärtner A, Ringstedt T, O'Leary DD (2004) EMX2 regulates sizes and positioning of the primary sensory and motor areas in neocortex by direct specification of cortical progenitors. *Neuron* 43:359–372.
- Harder L, Puller AC, Horstmann MA (2014) ZNF423: transcriptional modulation in development and cancer. *Mol Cell Oncol* 1:e969655.
- Hata A, Seoane J, Lagna G, Montalvo E, Hemmati-Brivanlou A, Massagué J (2000) OAZ uses distinct DNA- and protein-binding zinc fingers in separate BMP-Smad and Olf signaling pathways. *Cell* 100:229–240.
- Hill RE, Favor J, Hogan BL, Ton CC, Saunders GF, Hanson IM, Prosser J, Jordan T, Hastie ND, van Heyningen V (1991) Mouse small eye results from mutations in a paired-like homeobox-containing gene. *Nature* 354:522–525.
- Hong CJ, Hamilton BA (2016) Zfp423 regulates sonic hedgehog signaling via primary cilium function. *PLoS Genet* 12:e1006357.
- Ishino Y, et al. (2014) Bre1a, a histone H2B ubiquitin ligase, regulates the cell cycle and differentiation of neural precursor cells. *J Neurosci* 34:3067–3078.
- Kamiya D, et al. (2011) Intrinsic transition of embryonic stem-cell differentiation into neural progenitors. *Nature* 470:503–509.
- Kikkawa T, Obayashi T, Takahashi M, Fukuzaki-Dohi U, Numayama-Tsuruta K, Osumi N (2013) Dmrt1 regulates proneural gene expression downstream of Pax6 in the mammalian telencephalon. *Genes Cells* 18:636–649.

- Kircher M, Witten DM, Jain P, O'roak BJ, Cooper GM, Shendure J (2014) A general framework for estimating the relative pathogenicity of human genetic variants. *Nat Genet* 46:310–315.
- Konno D, Iwashita M, Satoh Y, Momiyama A, Abe T, Kiyonari H, Matsuzaki F (2012) The mammalian DM domain transcription factor *Dmrt2* is required for early embryonic development of the cerebral cortex. *PLoS One* 7:e46577.
- Konno D, Kishida C, Maehara K, Ohkawa Y, Kiyonari H, Okada S, Matsuzaki F (2019) *Dmrt* factors determine the positional information of cerebral cortical progenitors via differential suppression of homeobox genes. *Development* 146:dev174243.
- Ku M, Howard S, Ni W, Lagna G, Hata A (2006) OAZ regulates bone morphogenetic protein signaling through *Smad6* activation. *J Biol Chem* 281:5277–5287.
- Lee SM, Tole S, Grove EA, McMahon AP (2000) A local *Wnt-3a* signal is required for development of the mammalian hippocampus. *Development* 127:457–467.
- Leszczynski P, Śmiech M, Salam Teeli A, Haque E, Viger R, Ogawa H, Pierzchała M, Taniguchi H (2020) Deletion of the *Prdm3* gene causes a neuronal differentiation deficiency in P19 cells. *Int J Mol Sci* 21:7192.
- Li Z, et al. (2021) *Zfp521* is essential for the quiescence and maintenance of adult hematopoietic stem cells under stress. *iScience* 24:102039.
- Manuel M, et al. (2007) Controlled overexpression of *Pax6* in vivo negatively autoregulates the *Pax6* locus, causing cell-autonomous defects of late cortical progenitor proliferation with little effect on cortical arealization. *Development* 134:545–555.
- Manuel MN, Mi D, Mason JO, Price DJ (2015) Regulation of cerebral cortical neurogenesis by the *Pax6* transcription factor. *Front Cell Neurosci* 9:70.
- Maretto S, Cordenonsi M, Dupont S, Braghetta P, Broccoli V, Hassan AB, Volpin D, Bressan GM, Piccolo S (2003) Mapping *Wnt/β-catenin* signaling during mouse development and in colorectal tumors. *Proc Natl Acad Sci U S A* 100:3299–3304.
- Mariani J, et al. (2012) *Emx2* is a dose-dependent negative regulator of *Sox2* telencephalic enhancers. *Nucleic Acids Res* 40:6461–6476.
- Masserdotti G, Badaloni A, Song YS, Croci L, Barili V, Bergamini G, Vetter M, Consalez GG (2010) *ZFP423* coordinates notch and bone morphogenetic protein (BMP) signaling, selectively upregulating *Hes5* gene expression. *J Biol Chem* 285:30814–30824.
- Massimino L, Flores-Garcia L, Di Stefano B, Colasante G, Icoresi-Mazzeo C, Zaghi M, Hamilton BA, Sessa A (2018) *TBR2* antagonizes retinoic acid dependent neuronal differentiation by repressing *Zfp423* during corticogenesis. *Dev Biol* 434:231–248.
- Mayr C, et al. (2021) HDAC screening identifies the HDAC class I inhibitor romidepsin as a promising epigenetic drug for biliary tract cancer. *Cancers* 13:3862.
- McBride DJ, Buckle A, van Heyningen V, Kleinjan DA (2011) DNase hypersensitivity and ultraconservation reveal novel, interdependent long-range enhancers at the complex *Pax6* cis-regulatory region. *PLoS One* 6:e28616.
- Meier F, et al. (2018) Online parallel accumulation–serial fragmentation (PASEF) with a novel trapped ion mobility mass spectrometer. *Mol Cell Proteomics* 17:2534–2545.
- Mohammed H, Taylor C, Brown GD, Papachristou EK, Carroll JS, D'Santos CS (2016) Rapid immunoprecipitation mass spectrometry of endogenous proteins (RIME) for analysis of chromatin complexes. *Nat Protoc* 11:316–326.
- Monuki ES, Porter FD, Walsh CA (2001) Patterning of the dorsal telencephalon and cerebral cortex by a roof plate-*Lhx2* pathway. *Neuron* 32:591–604.
- Murphy MW, Zarkower D, Bardwell VJ (2007) Vertebrate DM domain proteins bind similar DNA sequences and can heterodimerize on DNA. *BMC Mol Biol* 8:1–14.
- Murphy MW, et al. (2015) An ancient protein-DNA interaction underlying metazoan sex determination. *Nat Struct Mol Biol* 22:442–451.
- Muzio L, Di Benedetto B, Stoykova A, Boncinelli E, Gruss P, Mallamaci A (2002a) *Emx2* and *Pax6* control regionalization of the pre-neuronogenic cortical primordium. *Cereb Cortex* 12:129–139.
- Muzio L, Di Benedetto B, Stoykova A, Boncinelli E, Gruss P, Mallamaci A (2002b) Conversion of cerebral cortex into basal ganglia in *Emx2*($-/-$) *Pax6* (Sey/Sey) double-mutant mice. *Nat Neurosci* 5:737–745.
- Nan X, Campoy FJ, Bird A (1997) *MeCP2* is a transcriptional repressor with abundant binding sites in genomic chromatin. *Cell* 88:471–481.
- Nitarska J, Smith JG, Sherlock WT, Hillege MM, Nott A, Barshop WD, Vashisht A, Wohlschlegel JA, Mitter R, Riccio A (2016) A functional switch of NuRD chromatin remodeling complex subunits regulates mouse cortical development. *Cell Rep* 17:1683–1698.
- Ochi S, Manabe S, Kikkawa T, Ebrahimiazar S, Kimura R, Yoshizaki K, Osumi N (2024) A transcriptomic dataset of embryonic murine telencephalon. *Sci Data* 11:586.
- Ohkubo N, et al. (2014) Abnormal behaviors and developmental disorder of hippocampus in zinc finger protein 521 (*ZFP521*) mutant mice. *PLoS One* 9:e92848.
- O'Leary DD, Sahara S (2008) Genetic regulation of arealization of the neocortex. *Curr Opin Neurobiol* 18:90–100.
- Pattabiraman K, et al. (2014) Transcriptional regulation of enhancers active in protodomains of the developing cerebral cortex. *Neuron* 82:989–1003.
- Pei Z, Wang B, Chen G, Nagao M, Nakafuku M, Campbell K (2011) Homeobox genes *Gsx1* and *Gsx2* differentially regulate telencephalic progenitor maturation. *Proc Natl Acad Sci U S A* 108:1675–1680.
- Perez-Riverol Y, et al. (2025) The PRIDE database at 20 years: 2025 update. *Nucleic Acids Res* 53:D543–D553.
- Petrich A, Nabhan C (2016) Use of class I histone deacetylase inhibitor romidepsin in combination regimens. *Leuk Lymphoma* 57:1755–1765.
- Pottmeier P, Nikolantonaki D, Lanner F, Peuckert C, Jazin E (2024) Sex-biased gene expression during neural differentiation of human embryonic stem cells. *Front Cell Dev Biol* 12:1341373.
- Reed GH, Kent JO, Wittwer CT (2007) High-resolution DNA melting analysis for simple and efficient molecular diagnostics. *Pharmacogenomics* 8:597–608.
- Richards S, et al. (2015) Standards and guidelines for the interpretation of sequence variants: a joint consensus recommendation of the American college of medical genetics and genomics and the association for molecular pathology. *Genet Med* 17:405–424.
- Sambrook J, Russell DW (2006) Purification of nucleic acids by extraction with phenol: chloroform. *CSH Protoc*.
- Sansom SN, Griffiths DS, Faedo A, Kleinjan DJ, Ruan Y, Smith J, van Heyningen V, Livesey FJ (2009) The level of the transcription factor *Pax6* is essential for controlling the balance between neural stem cell self-renewal and neurogenesis. *PLoS Genet* 5:e1000511.
- Saulnier A, et al. (2013) The doublesex homolog *Dmrt5* is required for the development of the caudomedial cerebral cortex in mammals. *Cereb Cortex* 23:2552–2567.
- Scardigli R, Bäumer N, Gruss P, Guillemot F, Le Roux I (2003) Direct and concentration-dependent regulation of the proneural gene *Neurogenin2* by *Pax6*. *Development* 130:3269–3281.
- Schaeren-Wiemers N, Gerfin-Moser A (1993) A single protocol to detect transcripts of various types and expression levels in neural tissue and cultured cells: in situ hybridization using digoxigenin-labelled cRNA probes. *Histochemistry* 100:431–440.
- Scicchitano S, et al. (2019) The stem cell-associated transcription co-factor, *ZNF521*, interacts with *GLI1* and *GLI2* and enhances the activity of the Sonic hedgehog pathway. *Cell Death Dis* 10:715.
- Shahbazi E, et al. (2016) Conversion of human fibroblasts to stably self-renewing neural stem cells with a single zinc-finger transcription factor. *Stem Cell Reports* 6:539–551.
- Shao M, Zhang Q, Truong A, Shan B, Vishvanath L, Li L, Seale P, Gupta RK (2021) *ZFP423* controls *EBF2* coactivator recruitment and

- PPAR γ occupancy to determine the thermogenic plasticity of adipocytes. *Genes Dev* 35:1461–1474.
- Shen S, Pu J, Lang B, McCaig CD (2011) A zinc finger protein Zfp521 directs neural differentiation and beyond. *Stem Cell Res Ther* 2:1–4.
- Sobreira N, Schiettecatte F, Valle D, Hamosh A (2015) GeneMatcher: a matching tool for connecting investigators with an interest in the same gene. *Hum Mutat* 36:928–930.
- Sun J, Rockowitz S, Xie Q, Ashery-Padan R, Zheng D, Cvekl A (2015) Identification of in vivo DNA-binding mechanisms of Pax6 and reconstruction of Pax6-dependent gene regulatory networks during forebrain and lens development. *Nucleic Acids Res* 43:6827–6846.
- Tole S, Hébert J (2020) Telencephalon patterning. In: *Patterning and cell type specification in the developing CNS and PNS* (Rubenstein J, Chen B, Kwan KY, Rakic P, eds), pp 23–48. Amsterdam: Academic press.
- Toresson H, Potter SS, Campbell K (2000) Genetic control of dorsoventral identity in the telencephalon: opposing roles for Pax6 and Gsh2. *Development* 127:4361–4371.
- Urquhart JE, et al. (2016) DMRTA2 (DMRT5) is mutated in a novel cortical brain malformation. *Clin Genet* 89:724–727.
- Van Lint C, Ghysdael J, Paras P Jr, Burny A, Verdin E (1994) A transcriptional regulatory element is associated with a nuclease-hypersensitive site in the pol gene of human immunodeficiency virus type 1. *J Virol* 68:2632–2648.
- Wilkinson DG, Nieto MA (1993) Detection of messenger RNA by in situ hybridization to tissue sections and whole mounts. *Methods Enzymol* 225:361–367.
- Yelagandula R, et al. (2023) ZFP462 safeguards neural lineage specification by targeting G9A/GLP-mediated heterochromatin to silence enhancers. *Nat Cell Biol* 25:42–55.
- Young FI, Keruzore M, Nan X, Gennet N, Bellefroid EJ, Li M (2017) The doublesex-related Dmrt2 safeguards neural progenitor maintenance involving transcriptional regulation of Hes1. *Proc Natl Acad Sci U S A* 114:E5599–E5607.
- Yousaf H, Fatima A, Ali Z, Baig SM, Toff M, Iqbal Z (2022) A novel non-sense variant in GRM1 causes autosomal recessive spinocerebellar ataxia 13 in a consanguineous Pakistani family. *Genes* 13:1667.
- Yousaf H, et al. (2023) A homozygous founder variant in PDE2A causes paroxysmal dyskinesia with intellectual disability. *Clin Genet* 104:324–333.
- Ypsilanti AR, et al. (2021) Transcriptional network orchestrating regional patterning of cortical progenitors. *Proc Natl Acad Sci U S A* 118:e2024795118.
- Ypsilanti AR, Rubenstein JL (2016) Transcriptional and epigenetic mechanisms of early cortical development: an examination of how Pax6 coordinates cortical development. *J Comp Neurol* 524:609–629.
- Yun K, Potter S, Rubenstein JL (2001) Gsh2 and Pax6 play complementary roles in dorsoventral patterning of the mammalian telencephalon. *Development* 128:193–205.
- Zembrzycki A, Chou SJ, Ashery-Padan R, Stoykova A, O’leary DD (2013) Sensory cortex limits cortical maps and drives top-down plasticity in thalamocortical circuits. *Nat Neurosci* 16:1060–1067.